Enhancing Timeliness in Asynchronous Vehicle Localization: A Signal-Multiplexing Network Measuring Approach

Hanying Zhao, *Member, IEEE*, Zijian Zhang, *Graduate Student Member, IEEE*, Lingwei Xu, *Graduate Student Member, IEEE*, Yu Wang, *Fellow, IEEE*, and Yuan Shen, *Senior Member, IEEE*

***Abstract*— Cooperation among entities within networks for information exchange and measurement is a promising paradigm for high-accuracy positioning in automated vehicles. However, due to imperfect clocks and inefficient wireless protocols, current cooperative positioning techniques have inadequate accuracy and timeliness. This paper presents a novel localization framework for connected automated vehicles (CAVs) capable of achieving high-accuracy relative positioning with high update rates. We design a signal-multiplexing network measuring (SNM) protocol to optimize the measurement update rates and propose new range estimations to achieve high-accuracy ranging against clock errors and mobility. Using range estimations, we develop a relative localization algorithm that leverages intra- and inter-node cooperation with coordinate reference alignment to reconstruct the geometric relationships among the nodes. Performance analyses and simulation results demonstrate that our method achieves high-accuracy positioning with timely updates, ensuring reliability and robustness in asynchronous vehicle localization.**

***Index Terms*— Mobile systems, cooperative localization, relative localization, network ranging and clock synchronization.**

I. Introduction

HIGH-PRECISION localization are critical to intelligent transportation systems, which influence driving safety, traffic congestion, and the functioning of many innovative applications such as autonomous driving [1], [2], [3]. The global positioning system (GPS) is the most popular positioning, navigation, and timing service provider. However, in GPS-challenged scenarios, including tunnels, undercover areas, and urban canyons, and in safety-critical situations such as collision avoidance and lane-level positioning [2], there is a lacking of positioning and timing service with centimeter-level localization accuracy, nanosecond-level synchronization precision, and millisecond-level response latency.

Manuscript received 30 May 2023; revised 18 November 2023 and 21 February 2024; accepted 1 May 2024. This work was supported in part by the National Natural Science Foundation of China under Grant 62271285, in part by Tsinghua University—Meituan Joint Institute for Digital Life, and in part by Shanghai AI Laboratory. The Associate Editor for this article was M. Nicoli. *(Corresponding author: Yuan Shen.)*

The authors are with the Department of Electronic Engineering and Beijing National Research Center for Information Science and Technology, Tsinghua University, Beijing 100084, China (e-mail: hying_zhao@tsinghua.edu.cn; zhangzj20@mails.tsinghua.edu.cn; xlw22@mails.tsinghua.edu.cn; yu-wang@tsinghua.edu.cn; shenyuan_ee@tsinghua.edu.cn).

Digital Object Identifier 10.1109/TITS.2024.3404784

Cooperation between vehicles and roadside infrastructures in information exchange and internal measuring is a promising solution to high-accuracy positioning in intelligent transportation systems. In cooperative intelligent transportation systems (C-ITSs), vehicles and other devices inside the networks measure relative distances and directions and exchange information with others, facilitated by the emergence of vehicle-to-vehicle (V2V) and vehicle-to-everything (V2X) technologies [2]. For C-ITSs to work, plenty of standards, projects, and platforms are developed to specify the ideal, and detailed discussions on the wireless technologies are presented in [3], [4], [5], [6], and [7]. Despite their potential, the accuracy and timeliness of current cooperative localization methods remain challenging; most methods are augmentations to GPS [8], [9], [10], [11], [12], and may not be applicable in GPS-challenged scenarios. Various attempts have been made to ameliorate performance from the perspective of cooperation mechanisms and information fusion [13], [14], [15], [16]. However, the fundamental shortcoming of wireless positioning and timing arises from the hardware of devices [2]. Affected by voltage changes, ambient temperatures, hardware aging, and other external factors, the clocks of different devices are asynchronous even with careful initial calibration. Two key factors must be taken into account: frequency deviations (drifts) and offsets [17], [18], [19], [20], [21]. Fixed time offsets associated with the clock boot time can be coordinated through round-trip time (RTT), while the clock drift issue is more complicated and rarely considered. For commercial crystal-quartz clock oscillators, the clock frequency deviation is typically tens of parts per million (ppm), which will trigger meter-level ranging errors in milliseconds. Thus, simple, efficient ways to achieve **clock synchronization** that coordinates clock frequency for centimeter-level localization and nanosecond-level timing are necessary.

A. Joint Clock Synchronization and Localization

Previous research has demonstrated various attempts at joint clock synchronization and localization [22], [23], [24], [25], [26], [27], [28], [29], [30], [31], [32], which can be categorized into measuring ToFs and measuring TDoFs. ToFs characterize the time taken by wireless signals from transmitters to receivers and commonly require double-sided

TABLE I
COMPARISON BETWEEN OUR WORK AND EXISTING WORKS

Ranging method	Mobile scenario	Transmission mode	ToF estimation	TDoF estimation
SDS-TWR [25], ADS-TWR [26], AltDS-TWR [27]		Unicast	✓	
MPLS [32]	✓	Unicast	✓	
S-TDOA [29], PER [30], Alt-PER [31]		Unicast		✓
SM-NR [35]		Broadcast	✓	✓
Proposed SNM	✓	Broadcast	✓	✓

transmission. By contrast, TDoF measures the difference between ToFs from multiple transmitters, where receivers do not need to transmit measuring signals. For ToF estimation, two-way ranging (TWR) methods that measure the RTT between transmitters and receivers are popular, including SDS-TWR [25], ADS-TWR [26], and alternative double-sided TWR (AltDS-TWR) [27]. Ranging error analyses and field tests have shown that AltDS-TWR in [27] is the most robust one for pairwise ToF estimation [28]. For TDoF estimation, there are S-TDOA [29], PER [30], and alternative passive extended ranging (Alt-PER) method in [31], among which the most popular one is PER [30].

The above methods focus on static scenarios; however, mobility in transportation systems poses severe challenges for clock synchronization and ranging. On one hand, mobility, coupled with clock errors, renders the classic TWR formulations ineffective. On the other hand, the mobility of vehicles makes accuracy sensitive to measurement update rates, especially in fast-moving scenarios [33], [34]. Two potential solutions have been proposed in the literature. The first one is the mobile pairwise least squares (MPLS) [32], which is the first work accounting for the nodes' mobility in clock modeling without a priori of mobility. Using timestamps generated by at least four signals and performing a least-square estimation, MPLS can estimate pairwise ToFs in dynamic scenarios. However, MPLS measures ToFs one-to-one, causing the signal overhead to scale quadratically with the number of nodes. In large-scale networks with multiple nodes, MPLS will either incur long latency or occupy a large amount of spectrum resources, which is unsatisfactory in congested and safety-critical transportation scenarios. The second solution is the signal-multiplexing network ranging (SM-NR) [35]. By replacing the conventional one-to-one mode with the one-to-many, SM-NR can update measurements at the cost of a linear signal overhead with the network scale. However, SM-NR does not consider the users' mobility. As a result, although SM-NR can ensure high measurement update rates, the accuracy of ToF/TDoF estimations suffers from a severe loss. Up to now, a joint clock synchronization and network ranging method, which has a high update rate and is robust to the influence of users' mobility, is still blank. Table I summarizes the major features of these existing works.

B. Main Contributions

In this paper, we propose a high-efficiency cooperative localization framework for asynchronous vehicles, as shown in Fig. 1, which achieves precise relative positioning and accurate clock synchronization with high measurement update rates, ensuring reliable and robust performance in dynamic scenarios. Our contributions are summarized as follows.

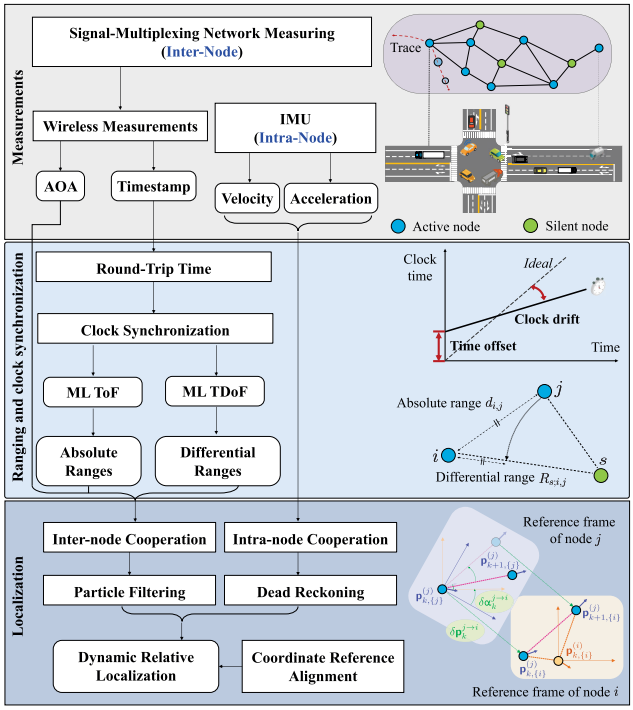

Fig. 1. Illustration of the proposed cooperative localization framework for positioning on connected automated vehicles.

- We establish a cooperative localization framework for CAVs, which ensures the timeliness and accuracy necessary for accommodating larger swarm sizes and fast-moving scenarios.
- We propose a SNM approach for vehicle positioning and clock synchronization, which reduces the measurement signal overhead from $\mathcal{O}(N^2)$ to $\mathcal{O}(N)$ in N-node networks. ToF and TDoF estimations are derived to achieve high-accuracy ranging with robustness to clock errors and vehicle mobility.
- We develop a relative localization algorithm that leverages both the intra-node and inter-node cooperation. Through the data fusion of network measuring and inertial measurement unit (IMU) sensing which incorporates coordinate reference alignment for robustness enhancement, the proposed algorithm can realize dynamic relative localization with high accuracy.

The rest of the paper is organized as follows. In Section II, we formulate the asynchronous vehicle localization problem. In Section III and Section IV, we present the designed network measuring protocol and the proposed ranging method. The timeliness and accuracy are then analyzed in Section V. In Section VI, we develop a cooperative relative localization algorithm by leveraging spatial-temporal cooperation.

Numerical simulation results are provided in Section VII, and conclusions are drawn in Section VIII.

Notation: Variables, vectors, and matrices are written as italic letters x, bold italic letters $\boldsymbol{x}$, and bold capital italic letters $\boldsymbol{X}$, respectively. Random variables, random vectors, and random matrices are denoted by sans serif letter x, bold letters $\mathbf{x}$, and bold capital letters $\mathbf{X}$, respectively. Letters with hats $\hat{(\cdot)}$ denote estimations; $\|\cdot\|$ denotes the Euclidean norm of its argument; $[\cdot]^{\mathrm{T}}$ represents the transpose of the argument.

II. Problem Formulation

A. Active-Silent Cooperative Localization Scheme

Consider an N-node transportation network, where a node can be a vehicle or any device that may affect or may be affected by, the vehicles. We propose a cooperative localization scheme designed to enhance the timeliness of asynchronous vehicle localization. This method optimizes the wireless measurement protocol, combines wireless measurements with IMU sensing, and can operate without relying on anchors.

Our method assigns N_{a} nodes working in active mode and N_{s} nodes working in silent mode, with $N_{\mathrm{a}} + N_{\mathrm{s}} = N$. Let $\mathcal{N}_{\mathrm{a}} \triangleq \{1, 2, \ldots, N_{\mathrm{a}}\}$ and $\mathcal{N}_{\mathrm{s}} \triangleq \{N_{\mathrm{a}}+1, \ldots, N_{\mathrm{a}}+N_{\mathrm{s}}\}$ denote the index sets of active and silent nodes, respectively, and $\mathcal{N} \triangleq \mathcal{N}_{\mathrm{a}} \cup \mathcal{N}_{\mathrm{s}}$. Active nodes will broadcast measuring signals, while silent nodes will only receive signals from the active ones. By designating a number of nodes to work in silent mode, we can reduce the signal overhead of wireless measurements and increase network capacity. Moreover, we will design methods that enable silent nodes to achieve ranging/localization accuracy comparable to that of active nodes, without the need for signal transmission.

1) Wireless Measurements: Wireless signals are transmitted, received, and processed to measure relative distances and directions between nodes. We define $\mathbf{z}_k^{(n)}$ to characterize the wireless measurements made by node n for the signal transmitted at discrete time instant k as[1]

$$\mathbf{z}_k^{(n)} = \begin{cases} [\mathsf{t}_k^{(n)} \quad \varphi_k^{(n)}]^{\mathrm{T}}, & \text{with arrays} \\ \mathsf{t}_k^{(n)}, & \text{without arrays} \end{cases} \tag{1}$$

where $\mathsf{t}_k^{(n)}$ represents the time of arrival (ToA) or time of departure (ToD) timestamp, and $\varphi_k^{(n)}$ denotes the angle of arrival (AoA). Here, time instant k refers to the period in which the k-th signal is emitted. Extensive research has been conducted on how to extract ToAs and AoAs from waveforms, such as [37], [38], and [39]. Since this topic is not the main focus of this paper, we do not discuss it in the following.

Time-based ranging metrics are adopted for ranging because they can provide high-resolution distance measurements. However, achieving this level of accuracy necessitates precise clock synchronization across different nodes, given that different clocks inevitably count time at different rates. According to [18], [19], [20], [21], [40], [41], and [42] and the IEEE 802.15.4a standard, the clock time of node n at time instant k can be modelled as:

$$\mathsf{t}_k^{(n)} = (1 + \mathsf{e}_k^{(n)}) t_k^{(n)} + \theta^{(n)}, \quad k = 1, 2, \ldots \tag{2}$$

where $\mathsf{t}_k^{(n)}$ and $t_k^{(n)}$ denote the observed timestamp and actural time, respectveily, and $\theta^{(n)}$ and $\mathsf{e}_k^{(n)}$ denote the time offset associated with the clock boot time and the clock frequency deviation, respectively. Follow the IEEE 802.15.4a standard, the clock frequency deviations $\mathsf{e}_k^{(n)}$ is modeled as independent normalized random variables bounded by $[-e_{\max}, +e_{\max}]$ [43], [44], [45]. Without careful calibration, these clock errors can lead to ranging errors of tens of meters. The goal of joint clock synchronization and ranging is to coordinate node clocks and extract high-accuracy ranging results from timestamp measurements.

2) IMU: In addition to wireless measurements, vehicles are also equipped with IMUs to acquire time-series velocity and acceleration information for positioning. Let $\mathbf{v}_k^{(n)}$ and $\mathbf{a}_k^{(n)}$ denote the velocity and the acceleration measurements obtained from the IMU of node n at discrete time instant k.

3) Spatial-Temporal Cooperation: Our localization scheme exploits inter-node cooperation by exchanging measurements via data communications. Specifically, node $n_1 \in \mathcal{N}$ can acquire the following elements from node $n_2 \in \mathcal{N} \backslash \{n_1\}$ for the purpose of information fusion in localization:

$$\mathcal{C}_k^{(n_2 \mapsto)} = \left\{ \mathbf{z}_k^{(n_2)}, \mathbf{v}_k^{(n_2)}, \mathbf{a}_k^{(n_2)} \right\}.$$

B. Relative Position Transformation

In transportation systems, to avoid collisions and manage traffic, we want to determine the relative geometric relationships among vehicles, other vehicles, and road infrastructures. To achieve this, we perform relative localization, in which the effects of translation, rotation, and reflection shall be eliminated and the relative relationships between nodes are recovered [15], [46], [47]. The detailed definitions of relative localization are as follows:

Given a position estimation $\hat{\mathbf{p}}$ of the network, the equivalent geometry of $\hat{\mathbf{p}}$ through transformation $\boldsymbol{\Psi} = \{\boldsymbol{\Gamma}, \boldsymbol{\nu}\}$ is defined as

$$S_{\boldsymbol{\Psi}}(\hat{\mathbf{p}}) = (\boldsymbol{I}_N \otimes \boldsymbol{\Gamma})\, \hat{\mathbf{p}} + \mathbf{1}_N \otimes \boldsymbol{\nu} \tag{3}$$

where $\boldsymbol{\Gamma} \in \mathcal{O}(2)$ is the orthogonal rotation (including reflection) matrix and $\boldsymbol{\nu} \in \mathbb{R}^2$ is the translation vector. In terms of relative localization, $S_{\boldsymbol{\Psi}}(\hat{\mathbf{p}})$ is considered to be geometrically equivalent to $\hat{\mathbf{p}}$. Then the relative position estimation corresponding to $\boldsymbol{p}$ is $\hat{\mathbf{p}}_{\mathrm{r}} = S_{\boldsymbol{\Psi}^*}(\hat{\mathbf{p}})$ where the optimal transformation parameter is

$$\boldsymbol{\Psi}^* = \arg\min_{\boldsymbol{\Psi}} \|\boldsymbol{p} - S_{\boldsymbol{\Psi}}(\hat{\mathbf{p}})\|^2 \tag{4}$$

which has a closed-form solution [15]. Therefore, the performance of relative localization of a network with N nodes can be evaluated by the normalized relative position error

$$\varepsilon_{\mathrm{r}} = \sqrt{\frac{1}{N} \left\| \hat{\mathbf{p}}_{\mathrm{r}} - \boldsymbol{p} \right\|^2}. \tag{5}$$

[1]The ranging principles we propose are also applicable in non-line-of-sight (NLOS) and multipath environments. The methods of extending these principles to such environments are demonstrated in our previous work [35], [36].

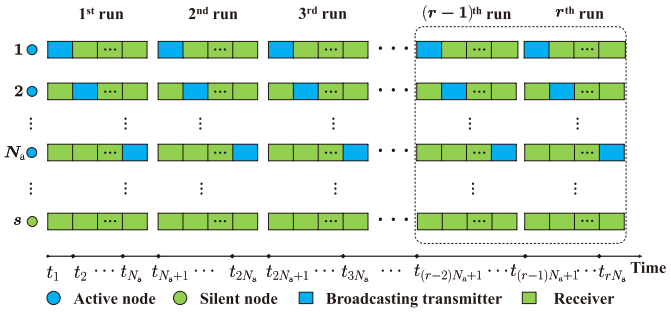

Fig. 2. Illustration of the protocol of SNM: active nodes recurrently broadcast signals for internal measuring, whereas silent nodes only receive.

III. Signal-Multiplexing Network Measuring

The mobility of vehicles imposes strict timeliness requirements on the measurement updates, especially in fast-moving scenarios. In this section, we optimize the network measuring protocol to provide the freshest information for ranging and positioning. We employ a broadcasting transmission mode for wireless measurements, in contrast to the unicasting mode commonly used in related works [25], [26], [27], [28], [29], [30], [31], [32]. With this transformation, we present a network measuring protocol via signal-multiplexing, where multiple TWR operations are conducted simultaneously. As analyzed in Section V, this protocol will significantly expedite the overall measuring process and enhance efficiency.

A. SNM Protocol

An illustration of the proposed SNM protocol is shown in Fig. 2. The order of measuring signal transmissions is preset. Without loss of generality, assume the signal transmission order follows the index number.

Recurrent Measuring: Active node 1 launches the network measuring process by transmitting the first measuring signal. Upon receiving this signal, active node 2 waits for a preset delay $I^{(2)}$ before transmitting the second signal. By analogy, each active node progressively emits measuring signals after its respective preset delays. Once active node N_a transmits its signal, we say one run of the network measuring process completes. A new run begins with active node 1 transmitting again after a delay of $I^{(1)}$. The initialization of SNM requires two rounds of signal transmission, with each active node transmitting twice in a sequential order.

In the r-th run when active node n ($n \in \mathcal{N}_\mathrm{a}$) is broadcasting, the index of time instant is $k = (r-1)N_\mathrm{a} + n$. SNM sets constant sending delays in different runs, i.e.,

$$t_k - t_{k-1} = \cdots = t_{k-(r-1)N_\mathrm{a}} - t_{k-(r-1)N_\mathrm{a}-1} = I^{(n)}. \tag{6}$$

The purpose of this design is to achieve clock synchronization, and a detailed explanation will be provided in Section IV-A.

B. Range Parameters

Let $\boldsymbol{p}_k^{(n)}$ denote the position of node n at time instant k. With timestamp measurements, one can determine *absolute ranges* and *differential ranges* for active and silent nodes, respectively, which are defined as follows:

- **Absolute ranges** are the ranges between two nodes. Let $d_k^{(i,j)}$ and $T_{\mathrm{oF}_k}^{(i,j)}$ respectively denote the absolute range and the ToF between nodes i and j at time instant k, which satisfies $d = cT_\mathrm{oF}$ where c is the signal transmission speed. The ToF is defined as

$$T_{\mathrm{oF}_k}^{(i,j)} := \frac{1}{c}\|\boldsymbol{p}_k^{(i)} - \boldsymbol{p}_k^{(j)}\| \tag{7}$$

- **Differential ranges** are range differences between node pairs. Consider silent-active node pairs (i,s) and (j,s), where node s is a silent node and nodes i and j are two active nodes. The differential range between them at time instant k is defined as

$$R_k^{(s;i,j)} = d_k^{(i,s)} - d_k^{(j,s)}$$

and satisfies $R^{(s;i,j)} := cT_\mathrm{R}^{(s;i,j)}$ with TDoF being defined as

$$T_{\mathrm{R}_k}^{(s;i,j)} := \frac{1}{c}\big[\|\boldsymbol{p}_k^{(i)} - \boldsymbol{p}_k^{(s)}\| - \|\boldsymbol{p}_k^{(j)} - \boldsymbol{p}_k^{(s)}\|\big] \tag{8}$$

and obeying $T_\mathrm{R}^{(s;i,j)} = T_\mathrm{oF}^{(i,s)} - T_\mathrm{oF}^{(j,s)}$.

Within an asynchronous network with N_a active nodes and N_s silent nodes, $\binom{N_\mathrm{a}}{2}$ absolute ranges among active nodes and $N_\mathrm{s}\binom{N_\mathrm{a}}{2}$ differential ranges can be determined:

$$\begin{aligned}\mathcal{D} &= \{d^{(i,j)} | \{i,j\} \subset \mathcal{N}_\mathrm{a}, \text{ and } i \neq j\}\\ \mathcal{R} &= \{R^{(s;i,j)} | s \in \mathcal{N}_\mathrm{s}, \ \{i,j\} \subset \mathcal{N}_\mathrm{a}, \text{ and } i \neq j\}.\end{aligned} \tag{9}$$

Here, we investigate fully-connected networks, where all nodes can receive every measuring signal. Our approach is also valid for partially connected networks, with the expansion process following the same principles presented in our earlier work [35], which is omitted due to space constraints.

The dynamic nature of vehicle networks necessitates the continual updating of the sets $\mathcal{D}$ and $\mathcal{R}$ in (9), **with the update frequency being a critical factor.** In SNM, during one transmission cycle, every range parameter in (9) will undergo two updates. Each measuring signal will do an update on $N_\mathrm{a}-1$ absolute ranges and $N_\mathrm{s}(N_\mathrm{a}-1)$ differential ranges associated with the transmitter. Specifically, when active node i broadcasts, the range parameters below will update,

$$\begin{aligned}\mathcal{D}_k &= \{d_k^{(i,j)} | j \in \mathcal{N}_\mathrm{a} \backslash \{i\}\}\\ \mathcal{R}_k &= \{R_k^{(s;i,j)} | s \in \mathcal{N}_\mathrm{s}, \ j \in \mathcal{N}_\mathrm{a} \backslash \{i\}\}.\end{aligned} \tag{10}$$

In Section V, we will show that SNM owns the highest measurement update rates in the state-of-the-art methods, thus providing the freshest information for ranging and positioning.

IV. Clock Synchronization and Network Ranging in Mobile Systems

To achieve robust range estimation, we propose a joint clock synchronization and network ranging strategy designed to solve the following ML problem:

$$\mathcal{D}_k^\star, \mathcal{R}_k^\star, \mathbf{e}^\star, \mathbf{v}_k^\star := \underset{\mathcal{D}_k, \mathcal{R}_k, \mathbf{e}, \boldsymbol{v}_k}{\operatorname{argmax}} \ \ell_\mathbf{e}(\mathcal{O}_k ; \mathcal{D}_k, \mathcal{R}_k, \mathbf{e}, \boldsymbol{v}_k) \tag{11}$$

where $\ell_\mathbf{e}(\cdot;\cdot)$ denotes the likelihood function with respect to frequency deviations $\mathbf{e} = [\mathrm{e}^{(1)} \ \mathrm{e}^{(2)} \ \cdots \ \mathrm{e}^{(N)}]^\mathrm{T}$, $\mathcal{O}_k = \{\mathrm{t}_m^{(n)} | 1 \le m \le k, \ n \in \mathcal{N}\}$ are timestamp observations, and $\boldsymbol{v}_k = [(\boldsymbol{v}_k^{(1)})^\mathrm{T} \ (\boldsymbol{v}_k^{(2)})^\mathrm{T} \ \cdots \ (\boldsymbol{v}_k^{(N)})^\mathrm{T}]^\mathrm{T}$ denotes velocity.

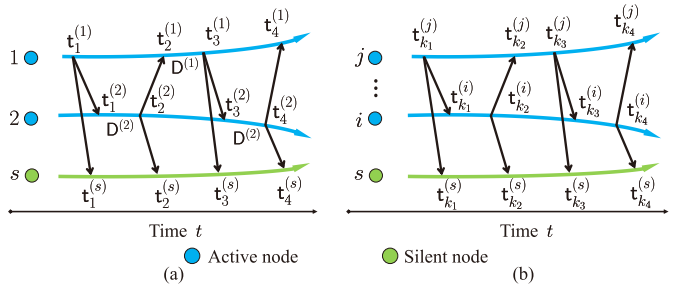

Fig. 3. Illustration of the timestamps captured by SNM, where the curved lines depict that the timestamps are influenced by both time-varying distances and clock drifts.

Solving (11) directly is difficult owing to its non-convex nature. To solve (11), our method first decouples mobility and clock errors, then achieves clock synchronization, and finally determines the time-varying ranges. For ease of illustration, we demonstrate the ranging method using 3-node cases in Section IV-A and extend it to network settings in Section IV-B.

A. ToF and TDoF Estimations

Taking active nodes 1 and 2 and silent node s as an illustration. We estimate $d_k^{(1,2)}$ and $R_k^{(s;1,2)}$ by calculating $T_{\mathrm{oF}_k}^{(1,2)}$ and $T_{\mathrm{R}_k}^{(s;1,2)}$, defined in (7) and (8), respectively. Considering $k = 4$ where each active node has transmitted twice and the timestamp measurements are $\mathcal{O}_4 = \{\mathsf{t}_k^{(n)} | 1 \le k \le 4, n = 1, 2, s\}$.

1) Mobility: As shown in Fig. 3, the TWR formulation for dynamic systems without clock errors can be described as

$$\begin{aligned} t_4^{(1)} - t_1^{(1)} - (t_4^{(2)} - t_1^{(2)}) &= T_{\mathrm{oF}_1}^{(1,2)} + T_{\mathrm{oF}_4}^{(1,2)} \\ t_3^{(2)} - t_2^{(2)} - (t_3^{(1)} - t_2^{(1)}) &= T_{\mathrm{oF}_2}^{(1,2)} + T_{\mathrm{oF}_3}^{(1,2)} \end{aligned} \tag{12}$$

where the RTTs on the left-hand side (LHS) and the ToFs on the right-hand side (RHS) are, respectively, what we measure and what we want. When nodes are mobile, the ToF at time instant 4 may differ from that at times 1 to 3, and then the unknown variables in (12) outnumber the equations, resulting in the failure of classical TWR methods. Although commercial IMUs on vehicles provide velocity information, their precision limitations can result in synchronization errors exceeding tens of nanoseconds and ranging errors exceeding tens of centimeters.

To enable ranging and clock synchronization in dynamic scenarios, we introduce an additional assumption to address the issue of having more unknowns than equations in (12). Allowed by the relationship between acceleration, measuring period, and ToF, we assume **uniform motion** between pairs within one ranging period. In this case, the relative velocity between nodes 1 and 2 is considered constant during the time interval (t_1, t_4). This assumption is reasonable because the average accelerations of commercial vehicles are typically less than five meters per second squared (depending on vehicle types), and the duration of one ranging period is around tens of milliseconds. The distance errors introduced by this uniform motion approximation are on the millimeter scale. Given that the accuracy of the best ToA techniques is at the centimeter level [48], [49], we believe such an approximation is close in practice.

Denoting the LHS of (12) as

$$\begin{aligned} \beta_1 &= t_4^{(1)} - t_1^{(1)} - (t_4^{(2)} - t_1^{(2)}) \\ \beta_2 &= t_3^{(2)} - t_2^{(2)} - (t_3^{(1)} - t_2^{(1)}) \end{aligned}$$

Applying the first-order Taylor expansion to (12), we obtain[2]

$$\begin{aligned} \beta_1 &\approx 2T_{\mathrm{oF}_4}^{(1,2)} - \frac{(\boldsymbol{p}_4^{(1)} - \boldsymbol{p}_4^{(2)})^{\mathrm{T}}}{\|\boldsymbol{p}_4^{(1)} - \boldsymbol{p}_4^{(2)}\|}(t_4^{(1)} - t_1^{(1)})\frac{\boldsymbol{v}_{1:4}^{(1,2)}}{c} \\ \beta_2 &\approx 2T_{\mathrm{oF}_4}^{(1,2)} - \frac{(\boldsymbol{p}_4^{(1)} - \boldsymbol{p}_4^{(2)})^{\mathrm{T}}}{\|\boldsymbol{p}_4^{(1)} - \boldsymbol{p}_4^{(2)}\|}(t_4^{(1)} - t_3^{(1)} + t_4^{(1)} - t_2^{(1)})\frac{\boldsymbol{v}_{1:4}^{(1,2)}}{c} \end{aligned} \tag{13}$$

where $\boldsymbol{v}_{1:4}^{(1,2)} := \boldsymbol{v}_{1:4}^{(1)} - \boldsymbol{v}_{1:4}^{(2)}$ denote the relative velocity between nodes 1 and 2 during the time interval $t \in (t_1, t_4)$. From (13), we can derive a ToF estimation that does not require knowledge of velocity, given by

$$T_{\mathrm{oF}_4}^{(1,2)} = \frac{\beta_1(2t_4^{(1)} - t_3^{(1)} - t_2^{(1)}) - \beta_2(t_4^{(1)} - t_1^{(1)})}{2(t_4^{(1)} - t_2^{(1)} + t_1^{(1)} - t_3^{(1)})}. \tag{14}$$

This ToF expression eliminates the necessity of knowing velocities, enabling us to extract ToFs directly from timestamp measurements. Next, we will elucidate the principle behind our ranging method for addressing clock errors.

2) Clock Synchronization: Due to the absence of a time server in the system, the vehicle system cannot ascertain the actual time for synchronization. Thus, we establish a **synchronization time**, which maintains a global average time as global time. Then, all node clocks stay synchronized with the synchronization time.

Definition 1: Synchronization time is defined as a function of timestamps, $T^{(n)} = f(\{t_k^{(n)}\})$, such that $T^{(1)} = T^{(2)}$.

Remark 1: When active nodes schedule signals to send by a fixed delay, $t_4^{(n)} - t_2^{(n)} + t_3^{(n)} - t_1^{(n)}$ can serve as a synchronization time for nodes 1 and 2. See Appendix A for a discussion of why such an expression $T^{(n)}$ can be used as a synchronization time.

Using synchronization time, we eliminate clock errors as follows. Recall the timestamp model in (2). The true values of timestamps are $\{t_k^{(n)}\}$ and we have $\{\mathsf{t}_k^{(n)}\}$ within clock errors in practice. We can eliminate both clock drifts and time offsets in $\mathsf{t}_k^{(n)} - \mathsf{t}_{k'}^{(n)}$ using the LHS operation described below:

$$\frac{T}{\mathsf{T}^{(n)}}(\mathsf{t}_k^{(n)} - \mathsf{t}_{k'}^{(n)}) = t_k^{(n)} - t_{k'}^{(n)}$$

where $T = T^{(1)} = T^{(2)}$, $\mathsf{T}^{(n)} = f(\{\mathsf{t}_k^{(n)}\})$ represents the synchronization time measurement at node n. Given that the actual synchronization time T is unknown, we derive an estimation, defined by

$$\widehat{\mathsf{T}}^{\star} = \underset{T}{\operatorname{argmax}}\ \ell_{\mathbf{e}}\left(\{\mathsf{t}_k^{(1)}\}_{k=1}^4, \{\mathsf{t}_k^{(2)}\}_{k=1}^4 ; T\right) \tag{15}$$

where $\mathbf{e} = [\mathsf{e}^{(1)}\ \mathsf{e}^{(2)}]^{\mathrm{T}}$. Then, we mitigate clock errors in $\mathsf{t}_k^{(n)} - \mathsf{t}_{k'}^{(n)}$ through the operation below

$$\frac{\widehat{\mathsf{T}}^{\star}}{\mathsf{T}^{(n)}}(\mathsf{t}_k^{(n)} - \mathsf{t}_{k'}^{(n)}) \tag{16}$$

[2]Given the nanosecond-level signal propagation time, we assume that node movements during signal transmission can be neglected, similar as MPLS in [32].

aligning node n with the synchronization time.

Remark 2: The exact expression of synchronization time estimation in (15) depends on the distribution of clock drift parameters, which highly depends on the physical characteristics of clocks. To explain (15), we take the uniform distribution as an example. When the clock frequency deviation is uniformly distributed in $[-e_{\max}, +e_{\max}]$, the estimation of T takes the form of $\widehat{\mathsf{T}}^{\star} = \max\left\{\mathsf{T}^{(1)}, \mathsf{T}^{(2)}\right\} / (1 + e_{\max})$.

3) ToF Estimation: We now have all the ingredients required to derive a ToF estimation that is robust to clock errors and node mobility. Using (14) along with (16) yields the proposition below.

Proposition 1: For the clock deviation parameter $\mathsf{e}^{(n)}$ with the probability density function (PDF) $h_{\mathsf{e}^{(n)}}(\cdot)$, an estimation of the ToF between nodes 1 and 2 at time instant 4 can be expressed as

$$\widehat{\mathsf{T}}_{\mathrm{oF}_4}^{(1,2)\star} = \frac{\beta_1(2\mathsf{t}_4^{(1)} - \mathsf{t}_3^{(1)} - \mathsf{t}_2^{(1)}) - \beta_2(\mathsf{t}_4^{(1)} - \mathsf{t}_1^{(1)})}{2(\mathsf{t}_4^{(1)} - \mathsf{t}_2^{(1)} + \mathsf{t}_1^{(1)} - \mathsf{t}_3^{(1)})} \tag{17}$$

where β_1 and β_2 are given by

$$\beta_1 = \frac{\widehat{\mathsf{T}}^{\star}}{\mathsf{T}^{(1)}}(\mathsf{t}_4^{(1)} - \mathsf{t}_1^{(1)}) - \frac{\widehat{\mathsf{T}}^{\star}}{\mathsf{T}^{(2)}}(\mathsf{t}_4^{(2)} - \mathsf{t}_1^{(2)})$$
$$\beta_2 = \frac{\widehat{\mathsf{T}}^{\star}}{\mathsf{T}^{(2)}}(\mathsf{t}_3^{(2)} - \mathsf{t}_2^{(2)}) - \frac{\widehat{\mathsf{T}}^{\star}}{\mathsf{T}^{(1)}}(\mathsf{t}_3^{(1)} - \mathsf{t}_2^{(1)})$$

in which $\widehat{\mathsf{T}}^{\star}$ is given in (15).

4) TDoF Estimation: Consider the TDoF estimation for silent node s. Using the same derivation method as in ToF estimation, we obtain the estimation of the TDoF.

Proposition 2: An estimation of the TDoF between active-silent pairs $(1, s)$ and $(2, s)$ at time instant 4 can be described as

$$\widehat{\mathsf{T}}_{\mathrm{R}_4}^{(s;1,2)\star} = \frac{\widehat{\mathsf{T}}^{\star}}{\mathsf{T}^{(2)}}(\mathsf{t}_4^{(2)} - \mathsf{t}_3^{(2)}) - \frac{\mathsf{t}_4^{(s)} - \mathsf{t}_3^{(s)}}{\mathsf{t}_3^{(s)} - \mathsf{t}_1^{(s)}} \cdot \frac{\widehat{\mathsf{T}}^{\star}}{\mathsf{T}^{(1)}}(\mathsf{t}_3^{(1)} - \mathsf{t}_1^{(1)}) + \widehat{\mathsf{T}}_{\mathrm{oF}_3}^{(1,2)\star} \tag{18}$$

where $\widehat{\mathsf{T}}^{\star}$ is given in (15) and $\widehat{\mathsf{T}}_{\mathrm{oF}_3}^{(1,2)\star}$ is the ToF estimation at time instant 3.

Proof: See Appendix B. □

B. Network Ranging and Clock Synchronization

We generalize the above ToF/TDoF estimations from 2-node cases to a network version.

As shown in Fig. 2, during the r-th run, when active node i broadcasts, we utilize the timestamps from the following time instants to estimate the ToF between active nodes i and j and the TDoF between the active-silent pairs (i, s) and (j, s):

$$k_1 = \begin{cases} k - (i - j) - N_{\mathrm{a}}, & \text{for } j < i \\ k + (j - i) - 2N_{\mathrm{a}}, & \text{for } j > i \end{cases} \tag{19}$$

$$k_3 = \begin{cases} k - (i - j), & \text{for } j < i \\ k + (j - i) - N_{\mathrm{a}}, & \text{for } j > i \end{cases} \tag{20}$$

$k_2 = k - N_{\mathrm{a}}$, and $k_4 = k$. The expressions for the ToF and the TDoF estimations are given below.

Proposition 3: A ToF estimation between nodes i and j at time instant k (k_4) when active node i broadcasts is given by

$$\widehat{\mathsf{T}}_{\mathrm{oF}_k}^{(i,j)\star} = \frac{\beta_1(2\mathsf{t}_{k_4}^{(j)} - \mathsf{t}_{k_3}^{(j)} - \mathsf{t}_{k_2}^{(j)}) - \beta_2(\mathsf{t}_{k_4}^{(j)} - \mathsf{t}_{k_1}^{(j)})}{2(\mathsf{t}_{k_4}^{(j)} - \mathsf{t}_{k_2}^{(j)} + \mathsf{t}_{k_1}^{(j)} - \mathsf{t}_{k_3}^{(j)})} \tag{21}$$

where

$$\beta_1 = \frac{\widehat{\mathsf{T}}^{\star}}{\mathsf{T}^{(j)}}(\mathsf{t}_{k_4}^{(j)} - \mathsf{t}_{k_1}^{(j)}) - \frac{\widehat{\mathsf{T}}^{\star}}{\mathsf{T}^{(i)}}(\mathsf{t}_{k_4}^{(i)} - \mathsf{t}_{k_1}^{(i)})$$
$$\beta_2 = \frac{\widehat{\mathsf{T}}^{\star}}{\mathsf{T}^{(i)}}(\mathsf{t}_{k_3}^{(i)} - \mathsf{t}_{k_2}^{(i)}) - \frac{\widehat{\mathsf{T}}^{\star}}{\mathsf{T}^{(j)}}(\mathsf{t}_{k_3}^{(j)} - \mathsf{t}_{k_2}^{(j)})$$

in which the synchronization time is fabricated as

$$\mathsf{T}^{(x)} \triangleq \mathsf{t}_{k_4}^{(x)} - \mathsf{t}_{k_2}^{(x)} + \mathsf{t}_{k_3}^{(x)} - \mathsf{t}_{k_1}^{(x)}, \quad \text{for } x = i, j \tag{22}$$

with estimation $\widehat{\mathsf{T}}^{\star} = \underset{T}{\operatorname{argmax}}\, \ell_{\mathsf{e}^{(i)},\mathsf{e}^{(j)}}\left(\mathsf{T}^{(i)}, \mathsf{T}^{(j)}; T\right)$. For silent node s, an estimation of the TDoF between active-silent pairs (i, s) and (j, s) obeys

$$\widehat{\mathsf{T}}_{\mathrm{R}_k}^{(s;i,j)\star} = \frac{\widehat{\mathsf{T}}^{\star}}{\mathsf{T}^{(j)}}(\mathsf{t}_{k_4}^{(j)} - \mathsf{t}_{k_3}^{(j)}) - \frac{\mathsf{t}_{k_4}^{(s)} - \mathsf{t}_{k_3}^{(s)}}{\mathsf{t}_{k_3}^{(s)} - \mathsf{t}_{k_1}^{(s)}} \frac{\widehat{\mathsf{T}}^{\star}}{\mathsf{T}^{(i)}}(\mathsf{t}_{k_3}^{(i)} - \mathsf{t}_{k_1}^{(i)}) + \widehat{\mathsf{T}}_{\mathrm{oF}_{k_3}}^{(i,j)\star}, \text{ when } j \text{ transmits.} \tag{23}$$

Proof: See Appendix C. □

Remark 3: We present a synchronization time that can coordinate the clocks of all nodes within the network for static scenarios in [35]. However, in dynamic scenarios, the mobility of nodes prevents the establishment of a global synchronization time. Thus, we are limited to coordinating the clocks of only two nodes.

According to (21) and (23), computing a ToF estimator requires six multiplication and three division operations, and computing a TDoF estimator requires nine multiplication and six division operations. Thus, in our distributed localization scheme, to acquire all $\binom{N_{\mathrm{a}}}{2}$ ToFs and $N_{\mathrm{s}}\binom{N_{\mathrm{a}}}{2}$ TDoFs, each node incurs a computational load of $4.5N_{\mathrm{a}}(N_{\mathrm{a}} - 1) + 7.5N_{\mathrm{s}}N_{\mathrm{a}}(N_{\mathrm{a}} - 1)$ FLOPS.[3] The computational complexity of other popular ranging methods can be found in [35, Table IV]. The computational complexity of the proposed method is low.

V. Performance Analysis

The performance of the proposed SNM method for joint clock synchronization and ranging in dynamic scenarios are analyzed with three benchmarks:

- **Benchmark 1** (AltDS-TWR [27]): The best-performed ToF estimation method in static scenarios [28], which measures one range using three measuring signals.
- **Benchmark 2** (MPLS [32]): A ToF estimation method for mobile scenarios, which measures one absolute range using M wireless measuring signals ($M \geq 4$).
- **Benchmark 3** (PER [30]): A popular TDoF estimation method. Note that PER needs to work with ToF estimation methods such as AltDS-TWR [27] and MPLS [32]. Here, we consider the combination of PER and AltDS-TWR.

[3]In a centralized localization manner, the center unit performs $4.5N_{\mathrm{a}}(N_{\mathrm{a}} - 1) + 7.5N_{\mathrm{s}}N_{\mathrm{a}}(N_{\mathrm{a}} - 1)$ FLOPS, without distributing them across individual nodes.

TABLE II
COMPARISON OF DIFFERENT NETWORK MEASURING SCHEMES FOR JOINT RANGING AND CLOCK SYNCHRONIZATION

Methods	Measurement update rates	Peak age of information	Worst-case errors
AltDS-TWR [27]	$1/3$	$(3\binom{N_a}{2}-1)I_{\max}$	$e_{\max}d^{(i,j)}_{k-(3\binom{N_a}{2}-1)}+(3\binom{N_a}{2}-1)I_{\max}v_{\max}$
MPLS [32]	$1/M$	$(M\binom{N_a}{2}-1)I_{\max}$	$\mathcal{O}(e_{\max}d^{(i,j)}_{k-(M\binom{N_a}{2}-1)})+(M\binom{N_a}{2}-1)I_{\max}v_{\max}$
PER [30]	$N_s/3$	$(3\binom{N_a}{2}-1)I_{\max}$	$e_{\max}c\left\|\delta^{(s)}_{i,j}-I_{\max}\right\|+e_{\max}c\left\|\delta^{(i)}_{i,j}-I_{\max}\right\|+(3\binom{N_a}{2}-1)I_{\max}v_{\max}$
Proposed SNM	$(N_s+1)(N_a-1)$	$(N_a-2)I_{\max}$	$\frac{2e_{\max}}{1+e_{\max}}d^{(i,j)}_{k-N_a+2}+(N_a-2)I_{\max}v_{\max}$

A. Efficiency

The measurement updates are desired to be as high as possible to provide the freshest information for ranging and positioning. We propose the following metrics to evaluate the timeliness of measuring methods.

Definition 2: Define the measurement update rate as the number of ToF and TDoF parameters that can be updated per measuring signal.

Definition 3: Define the peak age of information (PAoI) of the ToF/TDoF estimation as $\max_{k,k'}(t_k-t_{k'})$, where k and k' are the current time instant and the time instant of the last update, respectively. The notion of PAoI gauges the update interval and implicitly captures the freshness of measurements.

For ease of expression, we introduce the following notations. The maximal sending delay between two measuring signals is denoted as $I_{\max}$, which is typical at a ten-millisecond level. In one signal run, notation $\delta^{(n)}_{i,j}=t^{(n)}_j-t^{(n)}_i$ denotes the time interval made by node n between the measuring signals from active nodes i and j. Let $v_{\max}$ represent the maximum relative velocity value between two nodes.

Table II shows the update rates and peak age of information for different ranging schemes in a network with N_a active and N_s silent nodes. The proposed SNM achieves the highest update rate among state-of-the-art methods and delivers the freshest range information as it has the minimum peak age of ToF estimation. In dynamic environments, frequent updates of measurements ensure access to the freshest data, thus diminishing the ranging/localization errors incurred by outdated measurements. This efficiency enhancement originates from the optimized protocol that maximizes signal utilization. Such results indicate the usability and effectiveness of our ranging method for vehicular systems requiring low latency.

B. Effectiveness

Next, we analyze the range estimation error in dynamic systems. The ranging error between nodes i and j at the k-th time instant is defined as $\omega^{(i,j)}_k=\widehat{\mathsf{d}}^{(i,j)}_k-d^{(i,j)}_k$. Due to the combined impact of clock errors and vehicle mobility, ranging errors consist of two components: those arising from inaccuracies in ToF estimations and those from measurements that have become outdated. The proposition below characterizes the worst-case scenario for ToF estimation accuracy in the proposed SNM method. The accuracy of the TDoF within SNM is in the same order as ToF. Its analysis is omitted due to space constraints.

Proposition 4: The worst-case performance for the range estimation $\widehat{\mathsf{d}}^{(i,j)}_k$ of the SNM method can be described by

$$\max_{\mathbf{e}}\left\{\left|\omega^{(i,j)}_k\right|\right\}=\frac{2e_{\max}}{1+e_{\max}}d^{(i,j)}_{k-N_a+2}+(N_a-2)I_{\max}v_{\max}. \tag{24}$$

Proof: For the error induced by clock drifts, the worst-case performance can be characterized by the bound below

$$\begin{aligned}|\omega^{(i,j)}_k| &\overset{(a)}{=}\left|\frac{\underset{T}{\operatorname{argmax}}\prod_{n=1}^{2}h_{\mathsf{e}^{(n)}}(\mathsf{T}^{(n)};T)}{T}-1\right|d^{(i,j)}_k\\ &\overset{(b)}{\le}\frac{2e_{\max}}{1+e_{\max}}d^{(i,j)}_k\end{aligned} \tag{25}$$

where (a) elicits the range estimation error from clock drifts and inequality (b) is based on the clock frequency deviation parameter $\mathsf{e}^{(n)}$ which uniformly falls in the bounded interval $[-e_{\max},+e_{\max}]$. For the error induced by outdated measurements, we can derive it from the peak age of information, which gives the second term on the RHS of (24). □

The last column in Table II demonstrates the accuracy of different measuring schemes.[4] Compared with existing ranging methods, the SNM method provides the high-accuracy range results with the highest update rates. In networks with large N_a, it can be verified that the aging of information will become the dominant factor in range errors, which demonstrates the necessity of our effort to optimize the protocol to acquire the freshest information for ranging. In summary, our scheme eliminates the undesired effect of vehicle mobility, mitigates clock drifts, and boosts measuring update rates to decrease the ToF estimation error. To further verify the conclusion, numerical comparisons are shown in Section VII.

VI. COOPERATIVE LOCALIZATION IN DYNAMIC SCENARIOS

This section shows how to realize high-accuracy relative positioning on CAVs in a distributed way, which exploits

[4]The ToF of the MPLS is calculated through optimization without expressions. Numerical results in [32] show that the range error incurred by clock drifts grows linearly with $e_{\max}$.

intra- and inter-node cooperation with coordinate reference alignment to recover the geometric relationships.

A. Joint Network Localization Algorithm

The network relative position estimation can be initialized by the static relative localization algorithm in our previous work, where the multidimensional scaling (MDS)-based method and the Newton's method are adopted to minimize the least square cost function [35]. The main focus in this subsection is to realize distributed relative localization for dynamic scenes, in which we propose a scheme that combines particle filtering (PF) and dead reckoning (DR) to fuse the wireless signals and the IMU measurements for intra- and inter-node cooperation.[5]

Consider the general case where the network isn't fully-connected. Denote the neighbor sets that share LOS paths to node n as $\mathcal{N}^{(n)}$. At each time instant, the active nodes will broadcast their states and observations to the neighbors for cooperative localization. We denote the local state vector and the neighbor state vector of node n at time instant k as

$$\begin{aligned} \boldsymbol{x}_k^{(n)} &= \left[\boldsymbol{p}_k^{(n)\mathrm{T}}, \boldsymbol{v}_k^{(n)\mathrm{T}}, \boldsymbol{a}_k^{(n)\mathrm{T}}\right]^{\mathrm{T}}, \\ \boldsymbol{x}_{\mathcal{N},k}^{(n)} &= \left[\boldsymbol{p}_{\mathcal{N},k}^{(n)\mathrm{T}}, \boldsymbol{v}_{\mathcal{N},k}^{(n)\mathrm{T}}, \boldsymbol{a}_{\mathcal{N},k}^{(n)\mathrm{T}}\right]^{\mathrm{T}} \end{aligned} \tag{26}$$

where the position, velocity, and acceleration vector of node n's neighborhood $\mathcal{N}^{(n)}$ are $\boldsymbol{p}_{\mathcal{N},k}^{(n)} = \left[\boldsymbol{p}_k^{(j)\mathrm{T}}\right]_{j\in\mathcal{N}^{(n)}}^{\mathrm{T}}$, $\boldsymbol{v}_{\mathcal{N},k}^{(n)} = \left[\boldsymbol{v}_k^{(j)\mathrm{T}}\right]_{j\in\mathcal{N}^{(n)}}^{\mathrm{T}}$, and $\boldsymbol{a}_{\mathcal{N},k}^{(n)} = \left[\boldsymbol{a}_k^{(j)\mathrm{T}}\right]_{j\in\mathcal{N}^{(n)}}^{\mathrm{T}}$, respectively. Correspondingly, the absolute range measurements (for active node n) and the differential range measurements (for silent node m) in the neighborhood are denoted by $\mathbf{d}_{\mathcal{N},k}^{(n)} = \left[\widehat{\mathrm{d}}_k^{(n,j)}\right]_{j\in\mathcal{N}^{(n)}}^{\mathrm{T}}$ and $\mathbf{R}_{\mathcal{N},k}^{(m)} = \left[\widehat{\mathrm{R}}_k^{(m;i,j)}\right]_{i,j\in\mathcal{N}^{(m)}}^{\mathrm{T}}$, respectively. The IMU can provide measurements for the velocity and acceleration vector, $\mathbf{z}_{\mathcal{N},k}^{(n,\mathrm{IMU})} = \left[\mathbf{v}_k^{(n)\mathrm{T}}, \mathbf{v}_{\mathcal{N},k}^{(n)\mathrm{T}}, \mathbf{a}_k^{(n)\mathrm{T}}, \mathbf{a}_{\mathcal{N},k}^{(n)\mathrm{T}}\right]^{\mathrm{T}}$. Then we concatenate them as the complete neighborhood measurement vector for the active and silent nodes

$$\begin{aligned} \mathbf{z}_{\mathcal{N},k}^{(n)} &= \left[\mathbf{d}_{\mathcal{N},k}^{(n)\mathrm{T}}, \mathbf{z}_{\mathcal{N},k}^{(n,\mathrm{IMU})\mathrm{T}}\right]^{\mathrm{T}}, \ n \in \mathcal{N}_{\mathrm{a}}; \\ \mathbf{z}_{\mathcal{N},k}^{(m)} &= \left[\mathbf{R}_{\mathcal{N},k}^{(m)\mathrm{T}}, \mathbf{z}_{\mathcal{N},k}^{(m,\mathrm{IMU})\mathrm{T}}\right]^{\mathrm{T}}, \ m \in \mathcal{N}_{\mathrm{s}}. \end{aligned} \tag{27}$$

The goal of distributed dynamic relative localization for a node n is to estimate its local geometry $\left[\boldsymbol{p}_k^{(n)\mathrm{T}}, \boldsymbol{p}_{\mathcal{N},k}^{(n)\mathrm{T}}\right]^{\mathrm{T}}$ at each time instant k. Considering multi-sensory information fusion, since the IMU measurements usually have higher updating frequency than the wireless signals, we can perform the intact PF when both the wireless signals and the IMU measurements are available, and perform DR when only the IMU measurements are obtained, as shown in Fig. 4. The dynamic localization process is similar for both the active and silent nodes while only the observation models are different, and thus we won't distinguish between the mode of nodes in the following algorithm descriptions.

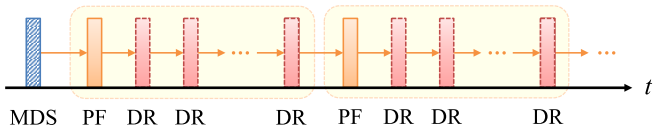

Fig. 4. The proposed dynamic relative localization framework that combines PF and DR.

For particle filtering, assign N_{p} particles for each node with particle states $\left\{\mathbf{x}_k^{(n,l)}\right\}_{l=1}^{N_{\mathrm{p}}}$ and weights $\left\{w_k^{(n,l)}\right\}_{l=1}^{N_{\mathrm{p}}}$. The state transition model and the observation model for PF are

$$\mathbf{x}_k^{(n,l)} = \boldsymbol{f}_k\left(\mathbf{x}_{k-1}^{(n,l)}\right) + \mathbf{n}_{\mathrm{state},k}^{(n,l)} \tag{28}$$

$$\mathbf{z}_{\mathcal{N},k}^{(n,l)} = \boldsymbol{h}_k\left(\mathbf{x}_k^{(n,l)}, \mathbf{x}_{\mathcal{N},k}^{(n,l)}\right) + \mathbf{n}_{\mathrm{obs},k}^{(n,l)} \tag{29}$$

where the state transition function $\boldsymbol{f}_k(\cdot)$ can be derived by time integration, the observation function $\boldsymbol{h}_k(\cdot)$ comes from the definitions of measurements, and the state transition noise $\mathbf{n}_{\mathrm{state},k}^{(n,l)} \sim \mathcal{N}\left(\mathbf{0}, \boldsymbol{Q}_k^{(n)}\right)$ and the observation noise $\mathbf{n}_{\mathrm{obs},k}^{(n,l)} \sim \mathcal{N}\left(\mathbf{0}, \boldsymbol{R}_k^{(n)}\right)$ are assumed Gaussian. Note that $\boldsymbol{f}_k(\cdot)$ and $\boldsymbol{h}_k(\cdot)$ could be time-variant due to the changeable link connections. The specific procedures of PF is standard and can refer to [50], which are omitted due to the limited space. After each round of particle filtering, the particle states and weights are updated, and the PF state estimation is obtained by

$$\widehat{\mathbf{x}}_k^{(n,\mathrm{PF})} = \sum_{l=1}^{N_{\mathrm{p}}} w_k^{(n,l)} \mathbf{x}_k^{(n,l)}. \tag{30}$$

For dead reckoning, the state transition model is similar to that of the PF model with the IMU measurements considered as the control vectors

$$\mathbf{x}_k^{(n,l)} = \boldsymbol{f}_k^{\mathrm{IMU}}\left(\mathbf{x}_{k-1}^{(n,l)}, \mathbf{z}_{k-1}^{(n,\mathrm{IMU})}\right) + \mathbf{n}_{\mathrm{state},k}^{(n,l)}. \tag{31}$$

During DR, we only update the particle states but leave their weights unchanged. The DR state estimation is simply derived from the state transition function

$$\widehat{\mathbf{x}}_k^{(n,\mathrm{DR})} = \boldsymbol{f}_k^{\mathrm{IMU}}\left(\widehat{\mathbf{x}}_{k-1}^{(n)}, \mathbf{z}_{k-1}^{(n,\mathrm{IMU})}\right). \tag{32}$$

In this way, the PF and DR process are combined to realize multi-source information fusion and obtain the local geometry estimation of each node in dynamic scenes.

Remark 4: In distributed relative localization, originally each node only derives the local geometry of its neighborhood. If the relative positions of the whole network is desired, geometry merging can be performed to broadcast and merge the local ones for the global estimation [51].

B. Coordinate Reference Alignment

In this subsection, we further consider the different characteristics between relative localization and absolute localization, and propose specific improvements to the algorithm above.

In distributed systems with harsh link connections, since each node actually performs the relative localization for the local geometry in its own coordinate reference frame, the coordinate datum of each node may differ, and can have cumulative drift over time due to the lack of absolute references.

[5]While some variants of Kalman Filter, e.g. Unscented Kalman Filter, are effective in the discussed scenario with less computational effort, we have chosen to apply PF for its high accuracy and versatility. Firstly, the dimension of the state vector is network scale-invariant, namely 6 in our case, and thus the computational burden of PF is tolerable in practical implementation and guarantees better accuracy. Secondly, PF can adapt to a range of models and noise distributions, allowing for the flexible customization of implementation details in various real-world application settings.

Thus directly utilizing the broadcasted neighbor states for particle filtering can lead to extra performance loss. To tackle this problem, we propose the coordinate reference alignment (CRA) scheme to calibrate the shared information from the neighbors and unify the local coordinate datum.

The general idea is that each node maintains a list of calibration parameters that characterize the difference between its own coordinate reference and each of its neighbor's

$$\boldsymbol{\Theta}_k^{(n)} = \left[\cdots \boldsymbol{\vartheta}_k^{j\to n} \cdots \right]_{j\in\mathcal{N}^{(n)}} \tag{33}$$

where the calibration parameter that transforms the coordinates from frame j to frame n is

$$\boldsymbol{\vartheta}_k^{j\to n} = \left[\delta\mathbf{p}_k^{j\to n\,\mathrm{T}}, \delta\alpha_k^{j\to n}, \mathbf{o}_k^{j\to n\,\mathrm{T}}\right]^{\mathrm{T}} \tag{34}$$

with rotation $\delta\alpha_k^{j\to n}$ around the center point $\mathbf{o}_k^{j\to n}$ and translation $\delta\mathbf{p}_k^{j\to n}$. The calibration parameters are updated alongside with the PF procedure, and thus the information shared between different coordinate reference frames can be aligned in real time.

Denote the estimated positions of node j in a certain reference frame i as $\widehat{\mathbf{p}}_{k,\{i\}}^{(j)}$. Then after receiving $\widehat{\mathbf{p}}_{k,\{j\}}^{(j)}$, node n can transform it from frame j to its own frame n by

$$\widetilde{\mathbf{p}}_{k,\{n\}}^{(j)} = \boldsymbol{R}(\delta\alpha_k^{j\to n})\left(\widehat{\mathbf{p}}_{k,\{j\}}^{(j)} - \mathbf{o}_k^{j\to n}\right) + \mathbf{o}_k^{j\to n} + \delta\mathbf{p}_k^{j\to n} \tag{35}$$

where $\boldsymbol{R}(\delta\alpha_k^{j\to n})$ is the rotation matrix with respect to $\delta\alpha_k^{j\to n}$. With such transformation, we can derive the calibrated neighbor state vector $\widetilde{\mathbf{x}}_{\mathcal{N},k,\{n\}}^{(n)}$, and then node n can perform PF precisely in its own coordinate reference frame.

The initialization for $\boldsymbol{\Theta}_0^{(n)}$ can be determined according to the initial localization results of the network. Then we consider the update for the calibration parameters. Utilizing the estimated $\widehat{\mathbf{x}}_k^{(n,\mathrm{PF})}$, we further perform backward calibration for the neighbor states, during which the neighbor state vector $\mathbf{x}_{\mathcal{N},k,\{n\}}^{(n)}$ is considered as the optimization variable, and $\widehat{\mathbf{x}}_k^{(n,\mathrm{PF})}$ is considered as the known parameter for the observation model of the current system. This can be achieved by least square optimization with the form

$$\widehat{\mathbf{x}}_{\mathcal{N},k,\{n\}}^{(n)} = \widetilde{\mathbf{x}}_{\mathcal{N},k,\{n\}}^{(n)} + \boldsymbol{K}_k^{(n)}\left(\mathbf{z}_{\mathcal{N},k}^{(n)} - \boldsymbol{H}_k^{(n)}\widetilde{\mathbf{x}}_{\mathcal{N},k,\{n\}}^{(n)}\right) \tag{36}$$

where $\boldsymbol{H}_k^{(n)}$ is the linear approximation matrix of the observation model, and $\boldsymbol{K}_k^{(n)}$ is the optimal coefficient matrix, the trivial details of which are omitted due to the limited space. Then $\boldsymbol{\Theta}_k^{(n)}$ can be updated according to the transformation from the original neighbor state $\mathbf{x}_{\mathcal{N},k,\{j\}}^{(n)}$ to the refined $\widehat{\mathbf{x}}_{\mathcal{N},k,\{n\}}^{(n)}$, which eliminates the cumulative drift between different coordinate reference frames.

By this refinement for the PF process, the distributed relative localization can be performed in a more robust and accurate manner, especially when a considerable number of communication links are disconnected. The complete procedure is summarized in Algorithm 1.

Remark 5: Note that we cannot simply incorporate the calibration parameters into the particle states for "joint estimation" in the context of relative localization. The challenge lies in the inability to achieve optimal state estimation by directly averaging the particle states (including node states and calibration parameters) in different reference frames, due to the absence of uniform coordinate datum. The optimal joint estimation needs further investigation.

Algorithm 1 Distributed Dynamic Network Localization for Active and Silent Nodes

Input: The neighborhood measurement vectors $\mathbf{z}_{\mathcal{N},k}^{(n)}, n \in \mathcal{N}, k = 1, 2, \ldots$

Output: Position estimations $\widehat{\mathbf{p}}_k^{(n)}, n \in \mathcal{N}, k = 1, 2, \ldots$

Initialize the relative position estimation $\widehat{\mathbf{p}}_0^{(n)}$ according to [35] and the calibration parameter $\boldsymbol{\Theta}_0^{(n)}$ $(n \in \mathcal{N})$;
Initialize the particle filter parameters $\left\{\mathbf{x}_0^{(n,l)}\right\}_{l=1}^{N_\mathrm{p}}$ and $\left\{w_0^{(n,l)}\right\}_{l=1}^{N_\mathrm{p}}$ for $n \in \mathcal{N}$;
for $k = 1, 2, \ldots,$ nodes $n \in \mathcal{N}$ in parallel **do**
  if complete observations $\mathbf{z}_{\mathcal{N},k}^{(n)}$ received **then**
    Perform CRA with calibration parameter $\boldsymbol{\Theta}_{k-1}^{(n)}$ by (35) to obtain the calibrated neighbor state $\widetilde{\mathbf{x}}_{\mathcal{N},k,\{n\}}^{(n)}$;
    Update the particle states according to the PF state transition model (28);
    Perform particle filtering and obtain $\widehat{\mathbf{p}}_k^{(n,\mathrm{PF})}$ by (30);
    Perform backward calibration by (36) and update $\boldsymbol{\Theta}_k^{(n)}$ accordingly;
  else if only IMU observations $\mathbf{z}_{k'}^{(n,\mathrm{IMU})}$ received **then**
    Update the particle states according to the DR state transition model (31);
    Perform dead reckoning and obtain $\widehat{\mathbf{p}}_{k'}^{(n,\mathrm{DR})}$ by (32);
  end if
end for
return Position estimations $\widehat{\mathbf{p}}_k^{(n)}, n \in \mathcal{N}, k = 1, 2, \ldots$

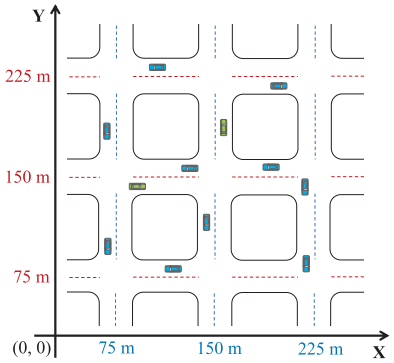

Fig. 5. The simulation scenario of a 300m×300m square plane, which includes three vertical roads and three horizontal roads.

Remark 6: With appropriate modifications, the proposed scheme can be extend to scenarios where absolute information is available. On the one hand, when anchor exists, the estimated network geometry can be transformed into absolute positions according to (4) by minimizing the absolute error with respect to the anchors. On the other hand, when absolute coordinate datum (e.g. GNSS signal) exists, we can modify the update manner of the calibration parameters to transform the local reference frames to the absolute reference frames.

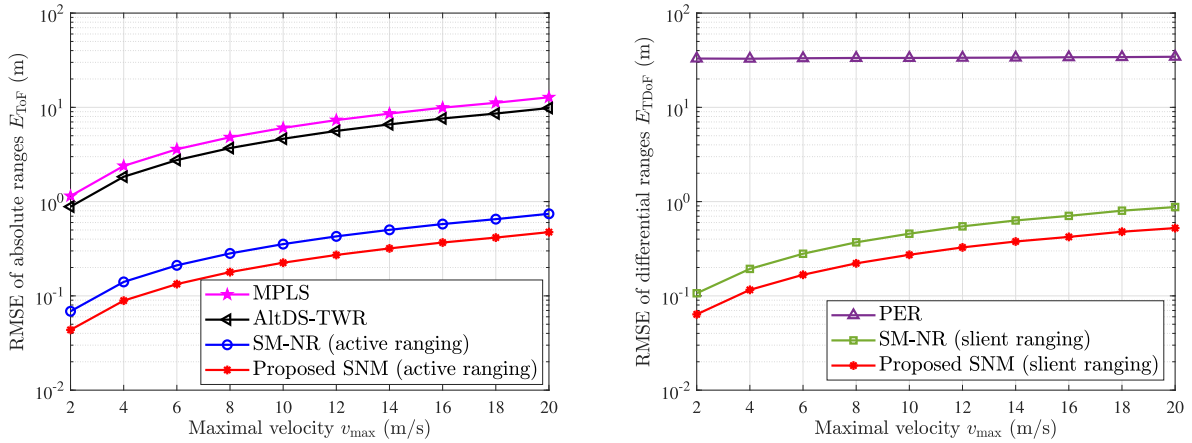

(a) ToF estimation performances (b) TDoF estimation performances

Fig. 6. The root mean square errors (RMSEs) of (a) absolute ranges and (b) differential ranges against the maximal velocity $v_{\max}$.

In summary, we establish a cooperative localization framework for asynchronous vehicle networks, which achieves high-accuracy relative positioning and clock synchronization by exploiting spatial-temporal cooperation in a distributed way. Particularly, we exploit the intra-node cooperation by incorporating IMU and wireless measurements, which refines nodes' states relative to those in previous instants. We reap the inter-node cooperation benefits through information exchange such that nodes aggregate more information for state updates. The cooperation scheme is distributed since, for practical implementation, distributed localization is more flexible, scalable, and safer as the nodes infer and refine states locally.

VII. Numerical Simulation Results

In this section, we numerically evaluate the effectiveness and efficiency of the proposed SNM method and the relative localization algorithm with four benchmarks. Except for AltDS-TWR [27], MPLS [32], and PER [30] aforementioned in Section V, our parallel work SM-NR [35], which is a hybrid of ToF and TDoF estimation method for static scenarios, is also compared. Starting from the $(N_{\mathrm{a}}+1)$-th time instant, SM-NR can update $\binom{N_{\mathrm{a}}}{2}$ absolute ranges and $N_{\mathrm{s}}\binom{N_{\mathrm{a}}}{2}$ differential ranges per time instant.

Unless particularly specified, we consider a 2-D scenario with $N_{\mathrm{a}}=10$ active nodes and $N_{\mathrm{s}}=2$ silent nodes, then there are $\binom{N_{\mathrm{a}}}{2}=45$ absolute ranges and $N_{\mathrm{s}}\binom{N_{\mathrm{a}}}{2}=90$ differential ranges to be measured. The initial positions of all nodes are randomly distributed on the nine roads of a 300 m $\times$300 m square plane [52], as shown in Fig. 5. The initial velocities of all nodes on the X-axis and Y-axis are both randomly distributed and always bounded by $[-v_{\max},+v_{\max}]$ with $v_{\max}=10$ m/s. The initial accelerated velocities of all nodes on the X-axis and Y-axis are randomly distributed in $[-a_{\max},+a_{\max}]$ with $a_{\max}=10$ m/s^2 and these accelerated velocities will randomly rebuild in each time instant to simulate the drivers' actions.

The total number of transmitted measuring signals (time instants) is $K=1000$, and the sending delays for each active node are all set to $I^{(n)}=10$ ms. The clock frequency deviations for all nodes are modeled as uniform random variables bounded by $[-e_{\max},+e_{\max}]$ with $e_{\max}=20$ ppm [28]. Each scheme holds its own absolute range set $\mathcal{D}$ and differential range set $\mathcal{R}$ in (10). Once the necessary timestamps for ranging have been collected, the range metrics will be updated. For the schemes requiring less number of ranging signals like SM-NR and the proposed SNM, the update frequency of their range measurements will be higher.

For the ranging part, all the simulation results in figures are the average results of 1000 independent experiments. The average RMSEs of all the absolute or differential ranges in $\mathcal{K}=\{1,2,\ldots,K\}$ time instants, denoted as E_{ToF} for absolute ranges and E_{TDoF} for differential ranges, are used as the performance metrics, respectively. For the localization part, we no longer distinguish between the active and silent modes, and adopt the performance metric of the relative RMSE normalized by the number of node in each local geometry for global performance evaluation, i.e., $E_{\mathrm{Loc}}=\mathbb{E}\left\{\sqrt{\frac{1}{KN}\sum_{k\in\mathcal{K}}\sum_{i\in\mathcal{N}}\epsilon_{\mathrm{r},i}^2[k]}\right\}$, where $\epsilon_{\mathrm{r},i}^2[k]$ is the averaged relative position error of the local geometry of node i estimated at the k-th time instant, as defined in (5).

A. RMSE of the SNM in Mobile Scenarios

We first evaluate the accuracy of various ranging schemes to verify the robustness of the proposed SNM against the user mobility. By jointly performing active and silent ranging methods, we plot the RMSEs of absolute ranges and differential ranges against the maximal velocity $v_{\max}$ in Fig. 6 (a) and Fig. 6 (b), respectively.

Firstly, the RMSEs of SM-NR and the proposed SNM are much lower than those of MPLS, AltDS-TWR, and PER. This is because the measurement update rates of SM-NR and SNM are much higher, thus reducing the ranging errors entailed by outdated measurements. For example, each signal in AltDS-TWR can only update 1/3 range since it requires 3 signals for estimating one absolute range. In contrast, after initialization, each signal in SM-NR will update 45 absolute ranges and 90 differential ranges, while each signal in SNM will update 9 absolute ranges and 18 differential ranges. The enhanced timeliness of wireless measurements provides the freshest measurements for ranging, and further improves the accuracy of vehicle localization in mobile scenarios.

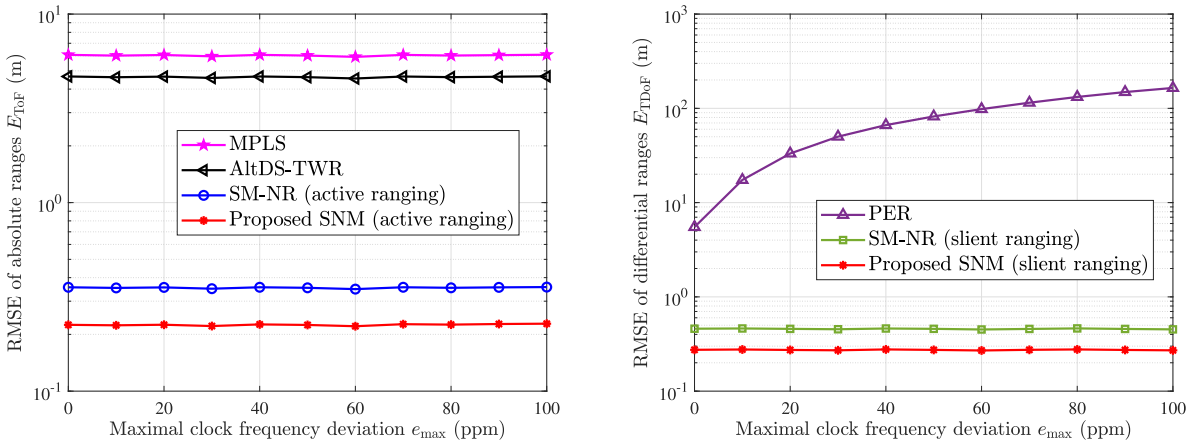

(a) ToF estimation performances (b) TDoF estimation performances

Fig. 7. The RMSEs of (a) absolute ranges; (b) differential ranges against the maximal clock frequency deviation $e_{\max}$.

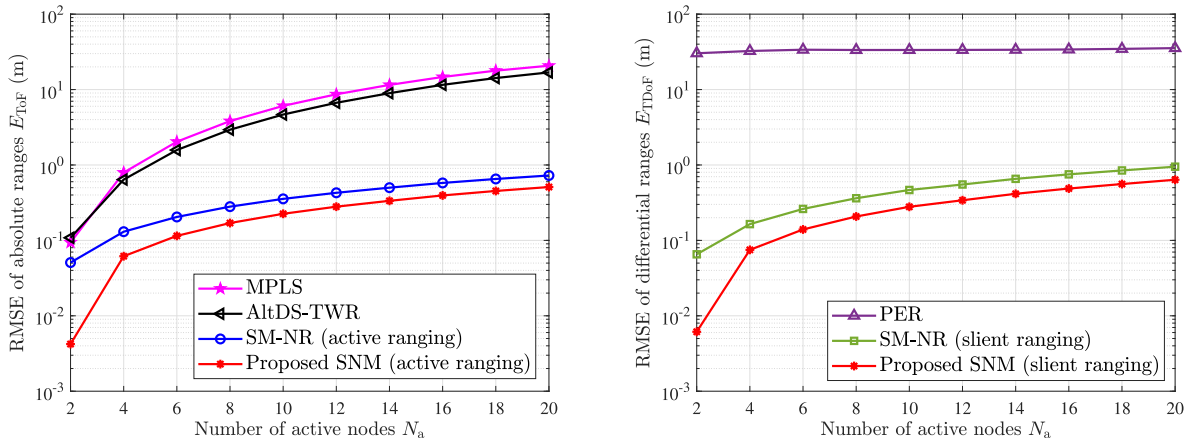

(a) ToF estimation performances (b) TDoF estimation performances

Fig. 8. The RMSE of (a) absolute ranges; (b) differential ranges against the number of active nodes, i.e., N_{a}.

Although SM-NR has higher measurement update rates than the proposed SNM, the accuracy of SM-NR is inferior to that of SNM in estimating ToF and TDoF. This is because SM-NR does not account for the impact of user mobility in RTT modeling, which leads to imprecise clock synchronization and inaccurate ranging results. In contrast, the proposed SNM incorporates the user mobility in RTT modeling and addresses the velocity-dependent terms in the estimation of ToFs and TDoFs, thus achieving a higher ranging accuracy than SM-NR.

B. RMSE of the SNM in the Presence of Clock Drifts

To verify the effective clock synchronization of the proposed SNM, we evaluate the impact of clock drifts on the ranging accuracy by plotting the RMSEs of absolute ranges and differential ranges against the maximal clock frequency deviation $e_{\max}$ in Fig. 7 (a) and Fig. 7 (b), respectively. Two figures show that as the clock drift effect becomes more significant, i.e., $e_{\max}$ becomes larger, the RMSEs of MPLS, AltDS-TWR, SM-NR, and the proposed SNM, nearly remain unchanged, while the RMSE of PER increases significantly. The reason for this phenomenon can be explained from two perspectives.

Firstly, with clock synchronization, MPLS, AltDS-TWR, SM-NR, and the proposed SNM for ToF estimation can almost eliminate the influence of clock errors on their ranging accuracy. Then, for these ranging methods, the low update rate replaces clock errors becoming the dominating factor in ranging accuracy, which finally determines their almost unchanged RMSEs. In contrast, PER does not effectively mitigate clock frequency deviations, leading to degraded ranging accuracy due to clock errors. As a result, the RMSE of PER increases rapidly with rising maximal clock frequency deviation $e_{\max}$ compared to our method for TDoF estimation. These results demonstrate the effective clock synchronization achieved by the proposed SNM.

C. RMSE of the SNM With Different Number of Active Nodes

Given 1000 time instants (i.e., transmitting 1000 measuring signals), Fig. 8 shows the RMSEs of ranging results as a function of the number of active nodes.

We observe that the RMSEs of all ranging methods rise with the increasing number of active nodes N_{a}. This occurs because the number of range parameters to be measured increases quadratically with N_{a}. Consequently, with a fixed number of measuring signals, the update frequency of each range parameter inevitably decreases as N_{a} increases. As a result, in dynamic scenarios, the RMSEs escalate with an increase in N_{a} due to untimely updates and outdated measurements. The growth rates of RMSEs reflect the scalability of the ranging methods. Fig. 8 shows that the proposed SNM and our

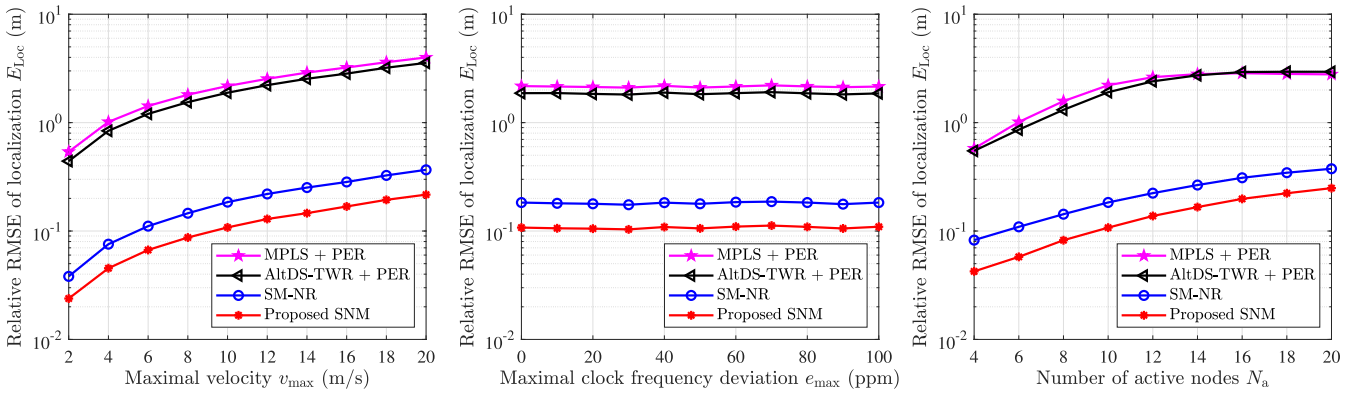

Fig. 9. The RMSE of relative position estimations against the maximal velocity, the maximal clock frequency deviation, and the number of active nodes.

former work SM-NR exhibit a smaller growth rate in RMSEs and lower RMSEs compared to other ranging methods. For example, in Fig. 8 (a), when $N_{\mathrm{a}} = 2$, the RMSEs of MPLS, AltDS-TWR, SM-NR, and SNM are 0.094 m, 0.108 m, 0.050 m, and 0.004 m, respectively. When $N_{\mathrm{a}} = 20$, these values are 20.71 m, 16.88 m, 0.725 m, and 0.510 m, respectively. These results indicate that in large-scale networks, the proposed SNM offers higher measurement update rates and achieves superior ranging accuracy, making it a preferable option for achieving high-accuracy localization.

D. RMSE of the Proposed Network Localization Algorithm

Finally, we evaluate the performance of the proposed network localization algorithm. Since relative localization involves the cooperation within the whole network, we consider the averaged RMSE of all nodes in the network, where both the ToF and the TDoF estimation results obtained by the methods in the previous subsections are considered as inputs of the localization system. Four typical combinations are considered, i.e., MPLS + PER, AltDS-TWR + PER, SM-NR, and the proposed SNM method.

The RMSEs of relative position estimations against the maximal velocity, the maximal clock frequency deviation, and the number of active nodes are shown in Fig. 9. Compared with Fig. 6, Fig. 7, and Fig. 8, we observe that the relative relations and the changing trends of the curves about localization are consistent with the performance of the range estimations. These results illustrate that the localization accuracy of the dynamic network critically depends on the ranging accuracy and demonstrate the accuracy and effectiveness of the proposed algorithms. On the other hand, the relative RMSEs of the localization results are about 40%∼60% lower than that of the ranging results in all scenarios, which reflects that the proposed cooperative localization scheme can mitigate the influence of measurement errors and improve the overall performance. Furthermore, the above results can provide helpful insights into improving the performance of the localization system by adjusting the network mobility, the quality of clock synchronization, and the network scale as well as the power management.

VIII. Conclusion

In this paper, we established a cooperative localization framework for positioning on CAVs, which has high measurement update rates and achieves high-accuracy positioning against clock errors in dynamic scenarios. The proposed SNM scheme consists of a signal-multiplexing network measuring protocol to enhance the timeliness of wireless measurements and new range estimations to mitigate the coupling effect of clock errors and vehicle mobility. Using range estimations, we develop a relative localization algorithm that leverages intra- and inter-node cooperation with coordinate reference alignment to reconstruct the geometric relationships among the nodes. Through the data fusion of network measuring and IMU sensing, the proposed algorithm can deliver enhanced robustness in achieving high-precision dynamic relative localization. Performance analyses and simulation results verified that our method achieves superior positioning performance in mobile systems, excelling in both accuracy and efficiency.

Appendix A
Discussion of Definition 1

As shown in Fig. 3(a), the relationship between positions and true values of timestamps can be described by (37). As active nodes send signals by a fixed delay, we have $t_4^{(2)} - t_3^{(2)} = t_2^{(2)} - t_1^{(2)} = I^{(2)}$. Then, applying the first-order Taylor expansion to (37) and using the uniform motion approximation, it follows that $(t_4^{(1)} - t_2^{(1)} + t_3^{(1)} - t_1^{(1)})/(t_4^{(2)} - t_2^{(2)} + t_3^{(2)} - t_1^{(2)}) \approx 1$. Thus, $t_4^{(n)} - t_2^{(n)} + t_3^{(n)} - t_1^{(n)}$ is approximately equal for $n = 1$ and $n = 2$, and can be used as a synchronization time.

$$t_3^{(1)} - t_1^{(1)} = \frac{1}{c}\Big[\|\boldsymbol{p}_2^{(1)} - \boldsymbol{p}_2^{(2)}\| + \|\boldsymbol{p}_1^{(1)} - \boldsymbol{p}_1^{(2)}\|\Big] + t_2^{(2)} - t_1^{(2)} + t_3^{(1)} - t_2^{(1)} \tag{37a}$$

$$t_4^{(1)} - t_2^{(1)} = \frac{1}{c}\Big[\|\boldsymbol{p}_4^{(1)} - \boldsymbol{p}_4^{(2)}\| + \|\boldsymbol{p}_3^{(1)} - \boldsymbol{p}_3^{(2)}\|\Big] + t_3^{(1)} - t_2^{(1)} + t_4^{(2)} - t_3^{(2)} \tag{37b}$$

$$t_3^{(2)} - t_1^{(2)} = \frac{1}{c}\Big[\|\boldsymbol{p}_3^{(1)} - \boldsymbol{p}_3^{(2)}\| + \|\boldsymbol{p}_2^{(1)} - \boldsymbol{p}_2^{(2)}\|\Big] + t_2^{(2)} - t_1^{(2)} + t_3^{(1)} - t_2^{(1)} \tag{37c}$$

$$t_4^{(2)} - t_2^{(2)} = \frac{1}{c}\Big[\|\boldsymbol{p}_3^{(1)} - \boldsymbol{p}_3^{(2)}\| + \|\boldsymbol{p}_2^{(1)} - \boldsymbol{p}_2^{(2)}\|\Big] + t_3^{(1)} - t_2^{(1)} + t_4^{(2)} - t_3^{(2)}. \tag{37d}$$

APPENDIX B
PROOF OF PROPOSITION 2

From Fig. 3(a), we obtain equations (38a) to (38c).

$$t_2^{(s)} - t_1^{(s)} + \frac{1}{c}\|\boldsymbol{p}_1^{(1)} - \boldsymbol{p}_1^{(s)}\| = \frac{1}{c}\Big[\|\boldsymbol{p}_1^{(1)} - \boldsymbol{p}_1^{(2)}\| + \|\boldsymbol{p}_2^{(2)} - \boldsymbol{p}_2^{(s)}\|\Big] + t_2^{(2)} - t_1^{(2)} \tag{38a}$$

$$t_3^{(s)} - t_2^{(s)} + \frac{1}{c}\|\boldsymbol{p}_2^{(2)} - \boldsymbol{p}_2^{(s)}\| = \frac{1}{c}\Big[\|\boldsymbol{p}_2^{(1)} - \boldsymbol{p}_2^{(2)}\| + \|\boldsymbol{p}_3^{(1)} - \boldsymbol{p}_3^{(s)}\|\Big] + t_3^{(1)} - t_2^{(1)} \tag{38b}$$

$$t_4^{(s)} - t_3^{(s)} + \frac{1}{c}\|\boldsymbol{p}_3^{(1)} - \boldsymbol{p}_3^{(s)}\| = \frac{1}{c}\Big[\|\boldsymbol{p}_3^{(1)} - \boldsymbol{p}_3^{(2)}\| + \|\boldsymbol{p}_4^{(2)} - \boldsymbol{p}_4^{(s)}\|\Big] + t_4^{(2)} - t_3^{(2)} \tag{38c}$$

where $\boldsymbol{v}_s$ denotes the relative velocity between node 2 and node s. Summing equations from (38a) to (38c), we have (38d).

$$t_4^{(s)} - t_1^{(s)} + \frac{1}{c}\|\boldsymbol{p}_1^{(1)} - \boldsymbol{p}_1^{(s)}\| = \frac{1}{c}\Big[\sum_{k=1}^{3}\|\boldsymbol{p}_k^{(1)} - \boldsymbol{p}_k^{(2)}\| + \|\boldsymbol{p}_4^{(2)} - \boldsymbol{p}_4^{(s)}\|\Big] + t_4^{(2)} - t_3^{(2)} + t_3^{(1)} - t_2^{(1)} + t_2^{(2)} - t_1^{(2)}. \tag{38d}$$

Applying the first-order Taylor expansion to (38c) and (38d) obeys (39).

$$t_4^{(s)} - t_3^{(s)} + T_{\mathrm{R}_4}^{(s;1,2)} \approx T_{\mathrm{oF}_3}^{(1,2)} + \frac{(\boldsymbol{p}_4^{(1)} - \boldsymbol{p}_4^{(s)})^{\mathrm{T}}}{\|\boldsymbol{p}_4^{(1)} - \boldsymbol{p}_4^{(s)}\|}(t_4^{(s)} - t_3^{(s)}) \cdot \frac{\boldsymbol{v}_{1:4}^{(1,2)} + \boldsymbol{v}_s}{c} + t_4^{(2)} - t_3^{(2)} \tag{39a}$$

$$t_4^{(s)} - t_1^{(s)} + T_{\mathrm{R}_4}^{(s;1,2)} \approx \sum_{k=1}^{3} T_{\mathrm{oF}_k}^{(1,2)} + \frac{(\boldsymbol{p}_4^{(1)} - \boldsymbol{p}_4^{(s)})^{\mathrm{T}}}{\|\boldsymbol{p}_4^{(1)} - \boldsymbol{p}_4^{(s)}\|}(t_4^{(s)} - t_1^{(s)}) \cdot \frac{\boldsymbol{v}_{1:4}^{(1,2)} + \boldsymbol{v}_s}{c} + t_4^{(2)} - t_3^{(2)} + t_3^{(1)} - t_2^{(1)} + t_2^{(2)} - t_1^{(2)} \tag{39b}$$

Combining (39a) and (39b) gives rise to (40), shown at the bottom of this page, which further yields the TDoF expression:

$$T_{\mathrm{R}_4}^{(s;1,2)} = T_{\mathrm{oF}_3}^{(1,2)} + (t_4^{(2)} - t_3^{(2)}) - \frac{t_4^{(s)} - t_3^{(s)}}{t_3^{(s)} - t_1^{(s)}}(t_3^{(1)} - t_1^{(1)}). \tag{41}$$

In the presence of clock errors, we mitigate clock errors through (16). Substituting the estimation of synchronization time into (41) yielding the TDoF estimation in (18).

APPENDIX C
PROOF OF PROPOSITION 3

Consider the ToF estimation between active nodes i and j. As shown in Fig. 3(b), the RTT and the ToFs satisfy

$$t_{k_4}^{(j)} - t_{k_1}^{(j)} - (t_{k_4}^{(i)} - t_{k_1}^{(i)}) = T_{\mathrm{oF}_{k_1}}^{(i,j)} + T_{\mathrm{oF}_{k_4}}^{(i,j)}$$
$$t_{k_3}^{(i)} - t_{k_2}^{(i)} - (t_{k_3}^{(j)} - t_{k_2}^{(j)}) = T_{\mathrm{oF}_{k_2}}^{(i,j)} + T_{\mathrm{oF}_{k_3}}^{(i,j)}.$$

Denoting the LHS of the above formulas as $\beta_1 = t_{k_4}^{(j)} - t_{k_1}^{(j)} - (t_{k_4}^{(i)} - t_{k_1}^{(i)})$ and $\beta_2 = t_{k_3}^{(i)} - t_{k_2}^{(i)} - (t_{k_3}^{(j)} - t_{k_2}^{(j)})$. Applying the first-order Taylor expansion, we have

$$\beta_1 \approx 2T_{\mathrm{oF}_{k_4}}^{(i,j)} - \frac{(\boldsymbol{p}_{k_4}^{(i)} - \boldsymbol{p}_{k_4}^{(j)})^{\mathrm{T}}}{\|\boldsymbol{p}_{k_4}^{(i)} - \boldsymbol{p}_{k_4}^{(j)}\|}\frac{\boldsymbol{v}_{k_1:k_4}^{(i,j)}}{c}(t_{k_4}^{(j)} - t_{k_1}^{(j)}) \tag{42}$$

$$\beta_2 \approx 2T_{\mathrm{oF}_{k_4}}^{(i,j)} - \frac{(\boldsymbol{p}_{k_4}^{(i)} - \boldsymbol{p}_{k_4}^{(j)})^{\mathrm{T}}}{\|\boldsymbol{p}_{k_4}^{(i)} - \boldsymbol{p}_{k_4}^{(j)}\|}\frac{\boldsymbol{v}_{k_1:k_4}^{(i,j)}}{c}(2t_{k_4}^{(j)} - t_{k_3}^{(j)} - t_{k_2}^{(j)})$$

where $\boldsymbol{v}_{k_1:k_4}^{(i,j)}$ denotes the relative velocity between nodes i and j during the time interval (t_{k_1}, t_{k_4}). Like the two-node cases, we can derive a ToF estimation that does not require knowledge of velocity from (42), given by:

$$T_{\mathrm{oF}_{k_4}}^{(i,j)} = \frac{\beta_1(2t_{k_4}^{(j)} - t_{k_3}^{(j)} - t_{k_2}^{(j)}) - \beta_2(t_{k_4}^{(j)} - t_{k_1}^{(j)})}{2(t_{k_4}^{(j)} - t_{k_2}^{(j)} + t_{k_1}^{(j)} - t_{k_3}^{(j)})}. \tag{43}$$

Next, we fabricate the synchronization time below to eliminate clock errors.

Remark 7: The term $T^{(n)} \triangleq t_{k_4}^{(n)} - t_{k_2}^{(n)} + t_{k_3}^{(n)} - t_{k_1}^{(n)}$ can be used a synchronization time.

We explain why $T^{(n)}$ can be used as a synchronization time. In the r-th run, when node i transmits, the constant sending delays described in (6) give rise to

$$\begin{aligned}
&|T^{(j)} - T^{(i)}|/T^{(j)} \\
&= |t_{k_4}^{(j)} - t_{k_4}^{(i)} - (t_{k_2}^{(j)} - t_{k_2}^{(i)}) + (t_{k_3}^{(j)} - t_{k_3}^{(i)}) - (t_{k_1}^{(j)} - t_{k_1}^{(i)})|/T^{(j)} \\
&= \Big|T_{\mathrm{oF}_{k_4}}^{(i,j)} - T_{\mathrm{oF}_{k_2}}^{(i,j)} - T_{\mathrm{oF}_{k_3}}^{(i,j)} + T_{\mathrm{oF}_{k_1}}^{(i,j)}\Big|/T^{(j)} \\
&\approx \Big|\frac{\|\boldsymbol{v}_{k_1:k_4}^{(i,j)}\|}{c}(t_{k_4} - t_{k_2} - (t_{k_3} - t_{k_1}))\Big|/T^{(j)} \\
&< (\frac{Q_{\max} - Q_{\min}}{2Q_{\min}})\frac{\|\boldsymbol{v}_{k_1:k_4}^{(i,j)}\|}{c}.
\end{aligned} \tag{44}$$

Here, $Q_{\min}$ and $Q_{\max}$ denote the minimum and maximum transmission durations for the i and j transmissions within the r-th run and the $(r-1)$-th run, respectively. As shown in Fig. 3(b), $Q_{\max} - Q_{\min}$ is smaller than the discrepancy in the total ToFs between the r-th run and the $(r-1)$-th run. Since the speed of light is substantially larger than vehicle speeds, and the difference in duration is less than the time taken for one run, $T^{(j)}$ can be viewed as approximately equal to $T^{(i)}$.

$$\frac{t_4^{(s)} - t_3^{(s)} + T_{\mathrm{R}_4}^{(s;1,2)} - T_{\mathrm{oF}_3}^{(1,2)} - (t_4^{(2)} - t_3^{(2)})}{t_4^{(s)} - t_1^{(s)} + T_{\mathrm{R}_4}^{(s;1,2)} - \sum_{k=1}^{3} T_{\mathrm{oF}_k}^{(1,2)} - (t_4^{(2)} - t_3^{(2)} + t_3^{(1)} - t_2^{(1)} + t_2^{(2)} - t_1^{(2)})} = \frac{t_4^{(s)} - t_3^{(s)}}{t_4^{(s)} - t_1^{(s)}} \tag{40}$$

Combing (43) and (22), the ToF estimation in (21) is obtained.

Next, consider the TDoF estimation among active nodes i, j and silent node s. When node j transmits, we have (45), given by

$$\begin{aligned}
&t_{k_4}^{(s)} - t_{k_3}^{(s)} + \frac{1}{c}\|\boldsymbol{p}_{k_3}^{(i)} - \boldsymbol{p}_{k_3}^{(s)}\| \\
&= \frac{1}{c}\Big[\|\boldsymbol{p}_{k_3}^{(i)} - \boldsymbol{p}_{k_3}^{(j)}\| + \|\boldsymbol{p}_{k_4}^{(j)} - \boldsymbol{p}_{k_4}^{(s)}\|\Big] + t_{k_4}^{(j)} - t_{k_3}^{(j)} \\
&t_{k_4}^{(s)} - t_{k_1}^{(s)} + \frac{1}{c}\|\boldsymbol{p}_{k_1}^{(i)} - \boldsymbol{p}_{k_1}^{(s)}\| \\
&= \frac{1}{c}\Big[\sum_{l=1}^{3}\|\boldsymbol{p}_{k_l}^{(i)} - \boldsymbol{p}_{k_l}^{(j)}\| + \|\boldsymbol{p}_{k_4}^{(j)} - \boldsymbol{p}_{k_4}^{(s)}\|\Big] \\
&\quad + t_{k_2}^{(j)} - t_{k_1}^{(j)} + t_{k_3}^{(i)} - t_{k_2}^{(i)} + t_{k_4}^{(j)} - t_{k_3}^{(j)}. \qquad (45)
\end{aligned}$$

Applying the first-order Taylor expansion on (45) and eliminating the velocities, the TDoF estimation can be described by

$$T_{\mathrm{R}_k}^{(s;i,j)} = T_{\mathrm{oF}_{k_3}}^{(i,j)} + t_{k_4}^{(j)} - t_{k_3}^{(j)} - \frac{t_{k_4}^{(s)} - t_{k_3}^{(s)}}{t_{k_3}^{(s)} - t_{k_1}^{(s)}}(t_{k_3}^{(i)} - t_{k_1}^{(i)}). \quad (46)$$

By substituting (22) into (46), we eliminate clock errors through the synchronization time and derive the TDoF estimation in (23), which completes the proof.

REFERENCES

[1] M. Z. Win, Y. Shen, and W. Dai, "A theoretical foundation of network localization and navigation," *Proc. IEEE*, vol. 106, no. 7, pp. 1136–1165, Jul. 2018.

[2] N. Alam and A. G. Dempster, "Cooperative positioning for vehicular networks: Facts and future," *IEEE Trans. Intell. Transp. Syst.*, vol. 14, no. 4, pp. 1708–1717, Dec. 2013.

[3] A. Festag, "Cooperative intelligent transport systems standards in Europe," *IEEE Commun. Mag.*, vol. 52, no. 12, pp. 166–172, Dec. 2014.

[4] S. Severi, H. Wymeersch, J. Harri, M. Ulmschneider, B. Denis, and M. Bartels, "Beyond GNSS: Highly accurate localization for cooperative-intelligent transport systems," in *Proc. IEEE Wireless Commun. Netw. Conf. (WCNC)*, Apr. 2018, pp. 1–6.

[5] K. Sjoberg, P. Andres, T. Buburuzan, and A. Brakemeier, "Cooperative intelligent transport systems in Europe: Current deployment status and outlook," *IEEE Veh. Technol. Mag.*, vol. 12, no. 2, pp. 89–97, Jun. 2017.

[6] J. Guerrero-Ibáñez, S. Zeadally, and J. Contreras-Castillo, "Sensor technologies for intelligent transportation systems," *Sensors*, vol. 18, no. 4, p. 1212, Apr. 2018.

[7] W. Li, Y. Liu, X. Li, and Y. Shen, "Three-dimensional cooperative localization via space-air-ground integrated networks," *China Commun.*, vol. 19, no. 1, pp. 253–263, Jan. 2022.

[8] N. Alam, A. Tabatabaei Balaei, and A. G. Dempster, "Relative positioning enhancement in VANETs: A tight integration approach," *IEEE Trans. Intell. Transp. Syst.*, vol. 14, no. 1, pp. 47–55, Mar. 2013.

[9] J. Liu, B.-G. Cai, and J. Wang, "Cooperative localization of connected vehicles: Integrating GNSS with DSRC using a robust cubature Kalman filter," *IEEE Trans. Intell. Transp. Syst.*, vol. 18, no. 8, pp. 2111–2125, Aug. 2017.

[10] K. Lassoued, P. Bonnifait, and I. Fantoni, "Cooperative localization with reliable confidence domains between vehicles sharing GNSS pseudoranges errors with no base station," *IEEE Intell. Transp. Syst. Mag.*, vol. 9, no. 1, pp. 22–34, Spring 2017.

[11] R. Kianfar et al., "Design and experimental validation of a cooperative driving system in the grand cooperative driving challenge," *IEEE Trans. Intell. Transp. Syst.*, vol. 13, no. 3, pp. 994–1007, Sep. 2012.

[12] M. Rohani, D. Gingras, V. Vigneron, and D. Gruyer, "A new decentralized Bayesian approach for cooperative vehicle localization based on fusion of GPS and VANET based inter-vehicle distance measurement," *IEEE Intell. Transp. Syst. Mag.*, vol. 7, no. 2, pp. 85–95, Summer 2015.

[13] S. Tang, N. Kubo, N. Kawanishi, R. Furukawa, A. Hasegawa, and Y. Takeuchi, "Cooperative relative positioning for intelligent transportation system," *Int. J. Intell. Transp. Syst. Res.*, vol. 13, no. 3, pp. 131–142, Sep. 2015.

[14] H. Li and F. Nashashibi, "Cooperative multi-vehicle localization using split covariance intersection filter," *IEEE Intell. Transp. Syst. Mag.*, vol. 5, no. 2, pp. 33–44, Summer 2013.

[15] Y. Liu, Y. Wang, J. Wang, and Y. Shen, "Distributed 3D relative localization of UAVs," *IEEE Trans. Veh. Technol.*, vol. 69, no. 10, pp. 11756–11770, Oct. 2020.

[16] S. S. Kia, S. Rounds, and S. Martinez, "Cooperative localization for mobile agents: A recursive decentralized algorithm based on Kalman-filter decoupling," *IEEE Control Syst. Mag.*, vol. 36, no. 2, pp. 86–101, Apr. 2016.

[17] Z. Zhang, H. Zhao, and Y. Shen, "High-efficient ranging algorithms for wireless sensor network," in *Proc. 11th Int. Conf. Wireless Commun. Signal Process. (WCSP)*, Xi'an, China, Oct. 2019, pp. 1–6.

[18] K.-L. Noh, E. Serpedin, and K. Qaraqe, "A new approach for time synchronization in wireless sensor networks: Pairwise broadcast synchronization," *IEEE Trans. Wireless Commun.*, vol. 7, no. 9, pp. 3318–3322, Sep. 2008.

[19] M. Ouellette, K. Ji, S. Liu, and H. Li, "Using IEEE 1588 and boundary clocks for clock synchronization in telecom networks," *IEEE Commun. Mag.*, vol. 49, no. 2, pp. 164–171, Feb. 2011.

[20] Y. Liu, Y. Shen, D. Guo, and M. Z. Win, "Network localization and synchronization using full-duplex radios," *IEEE Trans. Signal Process.*, vol. 66, no. 3, pp. 714–728, Feb. 2018.

[21] Y.-C. Wu, Q. Chaudhari, and E. Serpedin, "Clock synchronization of wireless sensor networks," *IEEE Signal Process. Mag.*, vol. 28, no. 1, pp. 124–138, Jan. 2011.

[22] Y. Wang, X. Ma, and G. Leus, "Robust time-based localization for asynchronous networks," *IEEE Trans. Signal Process.*, vol. 59, no. 9, pp. 4397–4410, Sep. 2011.

[23] P. Ferrari et al., "Timestamping and ranging performance for IEEE 802.15.4 CSS systems," *IEEE Trans. Instrum. Meas.*, vol. 63, no. 5, pp. 1244–1252, May 2014.

[24] C. L. Sang, M. Adams, T. Hörmann, M. Hesse, M. Porrmann, and U. Ruckert, "An analytical study of time of flight error estimation in two-way ranging methods," in *Proc. Int. Conf. Indoor Positioning Indoor Navigat. (IPIN)*, Nantes, France, Sep. 2018, pp. 1–8.

[25] H. Kim, "Double-sided two-way ranging algorithm to reduce ranging time," *IEEE Commun. Lett.*, vol. 13, no. 7, pp. 486–488, Jul. 2009.

[26] Y. Jiang and V. C. Leung, "An asymmetric double sided two-way ranging for crystal offset," in *Proc. Int. Symp. Signals, Syst. Electron.*, 2007, pp. 525–528.

[27] D. Neirynck, E. Luk, and M. McLaughlin, "An alternative double-sided two-way ranging method," in *Proc. 13th Workshop Positioning, Navigat. Commun. (WPNC)*, Oct. 2016, pp. 1–4.

[28] C. Lian Sang, M. Adams, T. Hörmann, M. Hesse, M. Porrmann, and U. Rückert, "Numerical and experimental evaluation of error estimation for two-way ranging methods," *Sensors*, vol. 19, no. 3, p. 616, Feb. 2019.

[29] M. Pelka and H. Hellbrück, "S-TDoA—Sequential time difference of arrival—A scalable and synchronization free approach forl positioning," in *Proc. IEEE Wireless Commun. Netw. Conf.*, Doha, Doha, Qatar, Apr. 2016, pp. 1–6.

[30] K. A. Horváth, G. Ill, and Á. Milánkovich, "Passive extended double-sided two-way ranging algorithm for UWB positioning," in *Proc. 9th Int. Conf. Ubiquitous Future Netw. (ICUFN)*, Milan, Italy, Jul. 2017, pp. 482–487.

[31] K. A. Horváth, G. Ill, and Á. Milánkovich, "Passive extended double-sided two-way ranging with alternative calculation," in *Proc. IEEE 17th Int. Conf. Ubiquitous Wireless Broadband (ICUWB)*, Sep. 2017, pp. 1–5.

[32] R. T. Rajan and A.-J. van der Veen, "Joint ranging and synchronization for an anchorless network of mobile nodes," *IEEE Trans. Signal Process.*, vol. 63, no. 8, pp. 1925–1940, Apr. 2015.

[33] E. Staudinger, S. Zhang, R. Pöhlmann, and A. Dammann, "The role of time in a robotic swarm: A joint view on communications, localization, and sensing," *IEEE Commun. Mag.*, vol. 59, no. 2, pp. 98–104, Feb. 2021.

[34] R. D. Yates, Y. Sun, and D. R. Brown, "Age of information: An introduction and survey," *IEEE J. Sel. Areas Commun.*, vol. 39, no. 5, pp. 1183–1210, Mar. 2021.

[35] Z. Zhang, H. Zhao, J. Wang, and Y. Shen, "Signal-multiplexing ranging for network localization," *IEEE Trans. Wireless Commun.*, vol. 21, no. 3, pp. 1694–1709, Mar. 2022.

[36] H. Zhao, Z. Zhang, J. Wang, Z. Zhang, and Y. Shen, "A signal-multiplexing ranging scheme for integrated localization and sensing," *IEEE Wireless Commun. Lett.*, vol. 11, no. 8, pp. 1609–1613, Aug. 2022.
[37] P. Stoica and A. Nehorai, "MUSIC, maximum likelihood, and cramer-rao bound," *IEEE Trans. Acoust., Speech, Signal Process.*, vol. 37, no. 5, pp. 720–741, May 1989.
[38] H. Zhao, N. Zhang, and Y. Shen, "Beamspace direct localization for large-scale antenna array systems," *IEEE Trans. Signal Process.*, vol. 68, pp. 3529–3544, 2020.
[39] H. Zhao, M. Huang, and Y. Shen, "High-accuracy localization in multipath environments via spatio-temporal feature tensorization," *IEEE Trans. Wireless Commun.*, vol. 21, no. 12, pp. 10576–10591, Dec. 2022.
[40] F. Lamonaca, A. Gasparri, E. Garone, and D. Grimaldi, "Clock synchronization in wireless sensor network with selective convergence rate for event driven measurement applications," *IEEE Trans. Instrum. Meas.*, vol. 63, no. 9, pp. 2279–2287, Sep. 2014.
[41] Y. Xiong, N. Wu, Y. Shen, and M. Z. Win, "Cooperative network synchronization: Asymptotic analysis," *IEEE Trans. Signal Process.*, vol. 66, no. 3, pp. 757–772, Feb. 2018.
[42] Q. Tian, D.-Z. Feng, H.-S. Hu, F. Yang, and L. Wei, "Bi-iterative algorithm for joint localization and time synchronization in wireless sensor networks," *Signal Process.*, vol. 154, pp. 304–313, Jan. 2019.
[43] *IEEE Standard for Local and Metropolitan Area Networks—Part 15.4: Low-Rate Wireless Personal Area Networks (LR-WPANs)*, IEEE Standard 802.15.4-2011, 2011.
[44] S. Wedge, "Predicting random jitter—Exploring the current simulation techniques for predicting the noise in oscillator, clock, and timing circuits," *IEEE Circuits Devices Mag.*, vol. 22, no. 6, pp. 31–38, Nov. 2006.
[45] S. P. Chepuri, R. T. Rajan, G. Leus, and A.-J. van der Veen, "Joint clock synchronization and ranging: Asymmetrical time-stamping and passive listening," *IEEE Signal Process. Lett.*, vol. 20, no. 1, pp. 51–54, Jan. 2013.
[46] J. N. Ash and R. L. Moses, "On the relative and absolute positioning errors in self-localization systems," *IEEE Trans. Signal Process.*, vol. 56, no. 11, pp. 5668–5679, Nov. 2008.
[47] X. Shen, L. Xu, Y. Liu, and Y. Shen, "A theoretical framework for relative localization," *IEEE Trans. Inf. Theory*, vol. 70, no. 1, pp. 735–762, Jan. 2024.
[48] M. Pan et al., "Efficient joint DOA and TOA estimation for indoor positioning with 5G picocell base stations," *IEEE Trans. Instrum. Meas.*, vol. 71, pp. 1–19, 2022.
[49] S. Gezici et al., "Localization via ultra-wideband radios: A look at positioning aspects for future sensor networks," *IEEE Signal Process. Mag.*, vol. 22, no. 4, pp. 70–84, Jul. 2005.
[50] F. Gustafsson et al., "Particle filters for positioning, navigation, and tracking," *IEEE Trans. Signal Process.*, vol. 50, no. 2, pp. 425–437, Feb. 2002.
[51] L. Xu, X. Shen, L. Wang, and Y. Shen, "A distributed relative localization scheme based on geometry merging priority," in *Proc. IEEE Global Commun. Conf.*, Rio de Janeiro, Brazil, Dec. 2022, pp. 3995–4000.
[52] H. Saleet, R. Langar, K. Naik, R. Boutaba, A. Nayak, and N. Goel, "Intersection-based geographical routing protocol for VANETs: A proposal and analysis," *IEEE Trans. Veh. Technol.*, vol. 60, no. 9, pp. 4560–4574, Nov. 2011.

Hanying Zhao (Member, IEEE) received the B.E. degree in information engineering from Xidian University, Xi'an, China, in 2016, and the Ph.D. degree in electronic engineering from Tsinghua University, Beijing, China, in 2021.

She is currently a Post-Doctoral Researcher with the Department of Electronic Engineering, Tsinghua University. Her research interests include statistical inference and network localization.

Zijian Zhang (Graduate Student Member, IEEE) received the B.E. degree in electronic engineering from Tsinghua University, Beijing, China, in 2020, where he is currently pursuing the Ph.D. degree in electronic engineering.

He is also an Amateur in wireless localization and robotics. He has authored or coauthored several journals and conference papers for the IEEE JOURNAL ON SELECTED AREAS IN COMMUNICATIONS, IEEE TRANSACTIONS ON SIGNAL PROCESSING, IEEE TRANSACTIONS ON WIRELESS COMMUNICATIONS, IEEE TRANSACTIONS ON COMMUNICATIONS, the IEEE ICC, and the IEEE GLOBECOM. His research interests include physical-layer algorithms for massive MIMO, holographic MIMO (H-MIMO), and reconfigurable intelligent surfaces (RIS). He has received the National Scholarship in 2019 and the Excellent Thesis Award of Tsinghua University in 2020.

Lingwei Xu (Graduate Student Member, IEEE) received the B.E. degree in electronic engineering from Tsinghua University, Beijing, China, in 2022, where he is currently pursuing the Ph.D. degree with the Department of Electronic Engineering.

His current research interests include relative localization and cooperative networks.

Yu Wang (Fellow, IEEE) received the B.S. and Ph.D. (Hons.) degrees from Tsinghua University, Beijing, in 2002 and 2007, respectively. He is currently a tenured Professor with the Department of Electronic Engineering, Tsinghua University. He has authored and co-authored more than 350 papers in refereed journals and conferences. His research interests include brain inspired computing, parallel circuit analysis, application specific acceleration and power/reliability aware circuit, and system design methodology. He has received four Best Paper Awards from leading conferences, including ASPDAC 2019 and FPGA 2017, and 11 Best Paper Nominations. He is a recipient of Alexander von Humboldt Fellowship (2019), DAC Under-40 Innovators Award (2018). He serves as an Associate Editor of the ACM TODAES and IEEE TCSVT. He also serves as TPC chair for ASP-DAC 2025, ICFPT 2019 and 2011, ISVLSI 2018, track chair for DAC 2022-2023, DATE 2017-2019, and GLSVLSI 2018.

Yuan Shen (Senior Member, IEEE) received the B.E. degree in electronic engineering from Tsinghua University in 2005 and the S.M. and Ph.D. degrees in electrical engineering and computer science from Massachusetts Institute of Technology (MIT) in 2008 and 2014, respectively.

He is currently a Full Professor with the Department of Electronic Engineering, Tsinghua University. His research interests include network localization and navigation, integrated sensing and control, and multi-agent systems. His papers have received the IEEE ComSoc Fred W. Ellersick Prize and several best paper awards from IEEE conferences. He has served as the TPC Symposium Co-Chair for IEEE ICC and IEEE Globecom for several times. He was the Elected Chair of the IEEE ComSoc Radio Communications Committee from 2019 to 2020. He is currently an Editor of the IEEE TRANSACTIONS ON SIGNAL PROCESSING, IEEE TRANSACTIONS ON COMMUNICATIONS, IEEE TRANSACTIONS ON NETWORK SCIENCE AND ENGINEERING, and *China Communications*.